nature cell biology

Apicobasal domain identities of expanding tubular membranes depend on glycosphingolipid biosynthesis

Hongjie Zhang[1], Nessy Abraham[1], Liakot A. Khan[1], David H. Hall[2], John T. Fleming[1] and Verena Göbel[1,3]

Metazoan internal organs are assembled from polarized tubular epithelia that must set aside an apical membrane domain as a lumenal surface. In a global *Caenorhabditis elegans* tubulogenesis screen, interference with several distinct fatty-acid-biosynthetic enzymes transformed a contiguous central intestinal lumen into multiple ectopic lumens. We show that multiple-lumen formation is caused by apicobasal polarity conversion, and demonstrate that *in situ* modulation of lipid biosynthesis is sufficient to reversibly switch apical domain identities on growing membranes of single post-mitotic cells, shifting lumen positions. Follow-on targeted lipid-biosynthesis pathway screens and functional genetic assays were designed to identify a putative single causative lipid species. They demonstrate that fatty-acid biosynthesis affects polarity through sphingolipid synthesis, and reveal ceramide glucosyltransferases (CGTs) as end-point biosynthetic enzymes in this pathway. Our findings identify glycosphingolipids, CGT products and obligate membrane lipids, as critical determinants of *in vivo* polarity and indicate that they sort new components to the expanding apical membrane.

Original inquiries into intrinsic polarizing components of membrane biogenesis[1] were superseded by the characterization of specific membrane-associated polarity molecules: plasma-membrane- and junction-associated protein complexes defining domain identities (identified by genetic morphogenesis screens in lower organisms); and endomembrane-based sorting signals directing transport (identified by the analysis of trafficking in mammalian cell lines)[2,3]. It is unclear how these distinct polarizing cues are integrated, how they themselves are regulated and how they relate to other polarity cues that arise during cell division, migration and tissue morphogenesis[4,5].

The limitation of genetic screens to identifying protein- or RNA-encoding genes may explain why lipids escaped numerous genetic screens instrumental in discovering *in vivo* core polarity determinants[6,7]. In contrast, membrane lipids, particularly phosphoinositides, are well-established *in vitro* sorting signals[8–10]. Glycosphingolipids (GSLs), similarly to phosphoinositides, are ubiquitous, asymmetrically assorted endo- and plasma-membrane lipids, but their polarity function is less clear *in vitro* and unknown *in vivo*. GSLs (with and without cholesterol) are thought to laterally self-assemble into membrane microdomains (rafts), and as such were implicated in the apical delivery of several molecules, particularly glycosylphosphatidylinositol (GPI)-anchored proteins, in mammalian cell lines[11–15]. A more general GSL role in partitioning apical proteins and lipids along endomembranes, originally proposed to generate polarity by segregating the GSL-rich apical plasma membrane domain, has not yet been demonstrated[16–18]. Studies are furthermore limited by uncertain effects of toxins and lipids used for the *in vitro* analysis of sphingolipids. Moreover, GSL-biosynthetic-enzyme knockouts, although demonstrating an essential GSL role *in vivo*, failed to confirm a polarity function[19]. The ability of GSLs to generate polarized plasma membrane domains is therefore uncertain and their essential role in development is unknown.

Here, a global *C. elegans* tubulogenesis screen, followed by targeted lipid-biosynthetic pathway screens, identifies GSLs, the CGT products, as a lipid species, whose loss, along with each of ten of its upstream biosynthetic enzymes, displaces apical domains on expanding membranes, generating multiple intestinal lumens. An unbiased genetic morphogenesis screen thus identifies a membrane lipid with an apical sorting function in mammalian cell lines as an apical domain identity cue during *de novo* membrane biogenesis of invertebrate tubular epithelia.

RESULTS

Interference with four distinct lipid-biosynthetic enzymes converts apicobasal polarity, generating lateral lumens

To examine tubulogenesis and lumen formation, a visual RNA interference (RNAi) screen was carried out using *C. elegans* engineered with ERM-1::GFP-labelled lumenal membranes (Methods). RNAi with all chromosome III genes ($N = 2{,}278$) revealed that most

[1]Department of Pediatrics, Massachusetts General Hospital and Harvard Medical School, Boston, Massachusetts 02114, USA. [2]Center for *C. elegans* Anatomy, Department of Neuroscience, Albert Einstein College of Medicine, Bronx, New York 10461, USA.
[3]Correspondence should be addressed to V.G. (e-mail: gobel@helix.mgh.harvard.edu)

Received 29 December 2010; accepted 28 July 2011; published online 18 September 2011; DOI: 10.1038/ncb2328

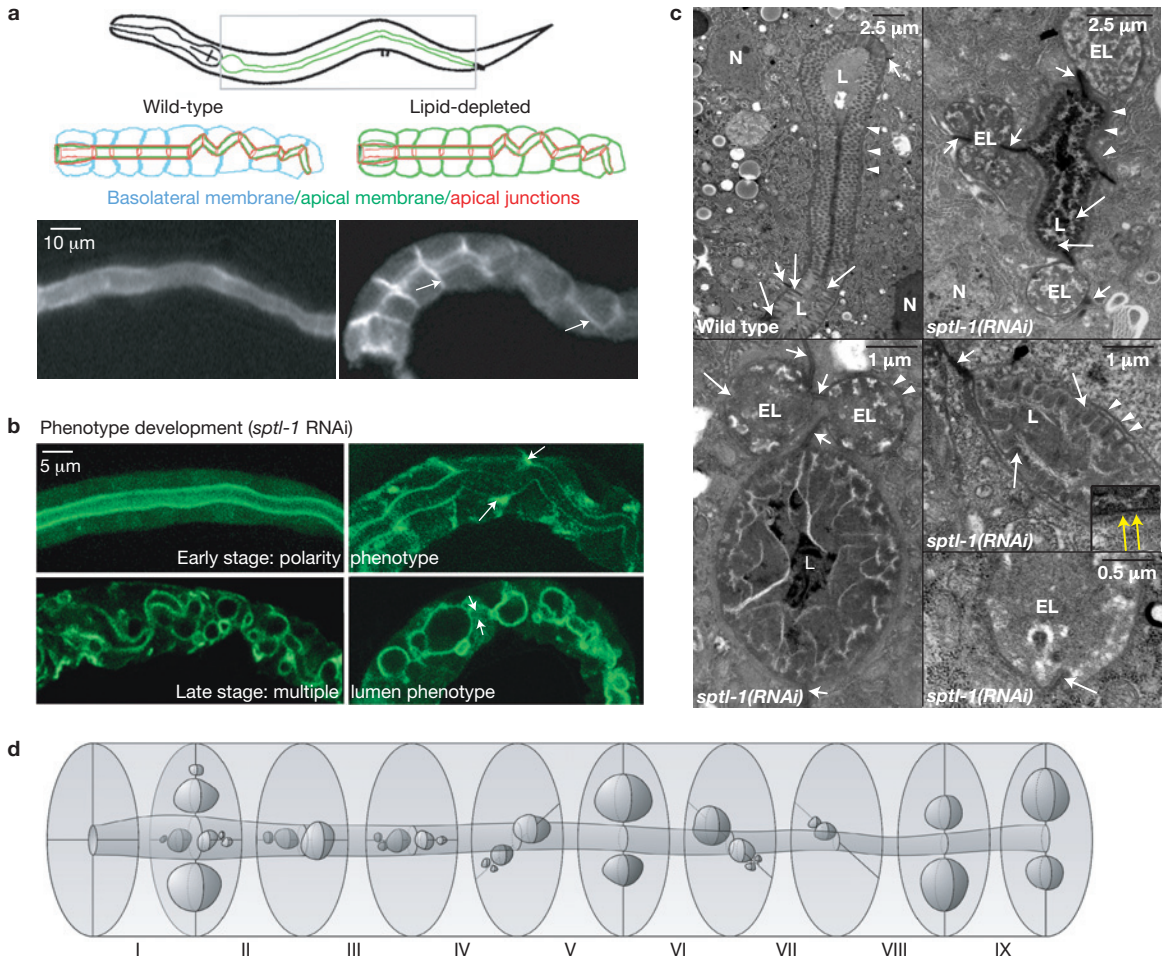

Figure 1 Apicobasal polarity conversion and ectopic lumen formation in the intestines of lipid-biosynthetic-enzyme-depleted animals. (See Supplementary Fig. S1 for anatomy and phenotypic details.) (**a**) Top, schematic representation of the mature single-layered *C. elegans* intestine where all apical membranes form the lumenal surface. The outlined area is magnified below. Bottom, epifluorescence dissecting micrographs of live animals (as identified in screen) showing displacement of the membrane–cytoskeleton linker ERM-1::GFP (ref. 57) from the apical (lumenal) membrane in wild type (left; for brevity, transgenic marker strains will be denoted as wild type) to the basolateral membrane in lipid-biosynthetic-enzyme-depleted animal (right; left arrow: lateral side, right arrow: basal side; note wild-type intercalation pattern). Representative *sptl-1(RNAi)* L1 are shown; *pod-2-, let-767-* and *acs-1* RNAi copy the phenotype (Supplementary Fig. S1b). Here and below, standard RNAi conditions (Methods) are shown unless indicated otherwise; anterior is left and dorsal up. (**b**) Typical phenotype development in RNAi L1 larvae. Confocal microscopy sections showing initial wild-type ERM-1::GFP placement (top left); ERM-1::GFP decrease from apical, and displacement to basolateral, membranes and enrichment in apicolateral angles (arrows; top right); multiple small lateral ectopic lumens (bottom left); ERM-1::GFP fully displaced from the central lumen to large lateral ectopic lumens (bottom right, arrows bracket central lumen area where ERM-1::GFP is missing). (**c**) TEM micrographs of intestinal cross-sections of wild-type (top left) and *sptl-1(RNAi)* L1 larvae (all others). Oval lumen (L) with dense microvilli (long white arrows) and tightly adjacent terminal web (arrowheads) in wild-type; deformed main lumen in RNAi animals with either short (long white arrows) or absent microvilli (right-middle inset, yellow arrows), dehiscence of the terminal web (arrowheads) and ectopic lateral lumens (EL) with stunted microvilli (long white arrows). Intact apical junctions (short arrows) in both wild-type and RNAi animals; note excess junctions between ectopic lateral lumens in RNAi animals; N, nucleus. Upper right image shows INT I. (**d**) Model of the multiple-lumen intestinal phenotype. Early ectopic lumen development (**b**, bottom-left image) in otherwise wild-type intestine is shown. Twenty intestinal cells are arranged in bilateral symmetry to form nine INT rings (I—IX; INT I contains four cells); rings twist along the anterior–posterior axis. View is from the anterior left lateral aspect[58].

(>90%) informative phenotypes involved essential genes, to which further genome screening was then restricted. A highly penetrant intestinal polarity phenotype (Fig. 1a) was identified by knockdowns of each of four different lipid-biosynthetic enzymes: POD-2, an acetyl-CoA carboxylase; LET-767, a steroid dehydrogenase/3-ketoacyl-CoA reductase; ACS-1, a long-chain-fatty-acid (LCFA)–acyl-CoA ligase; and SPTL-1, a serine palmitoyltransferase (SPT). Single-cell analysis of intestinal tubulogenesis revealed the same sequence of events in all: in either late-stage embryos (*pod-2(RNAi)*) or first-stage larvae (L1; *let-767, acs-1-* and *sptl-1(RNAi)*, their respective arrest stages) ERM-1::GFP was gradually lost from the apical membrane while appearing at basolateral membranes; lateral membranes transformed into ring structures; initially contiguous central apical ERM-1::GFP fractionated into non-contiguous lateral openings, indicating that multiple lateral ectopic lumens may be present (Fig. 1b and Supplementary Fig. S1a,b). Digestive tract morphogenesis appeared otherwise unaffected and the epithelium intact (Supplementary Fig. S2).

Additional apical submembraneous and integral membrane proteins were all similarly displaced to lateral membranes or the cytoplasm, including cortical actin and the apical Par (partitioning-defective)

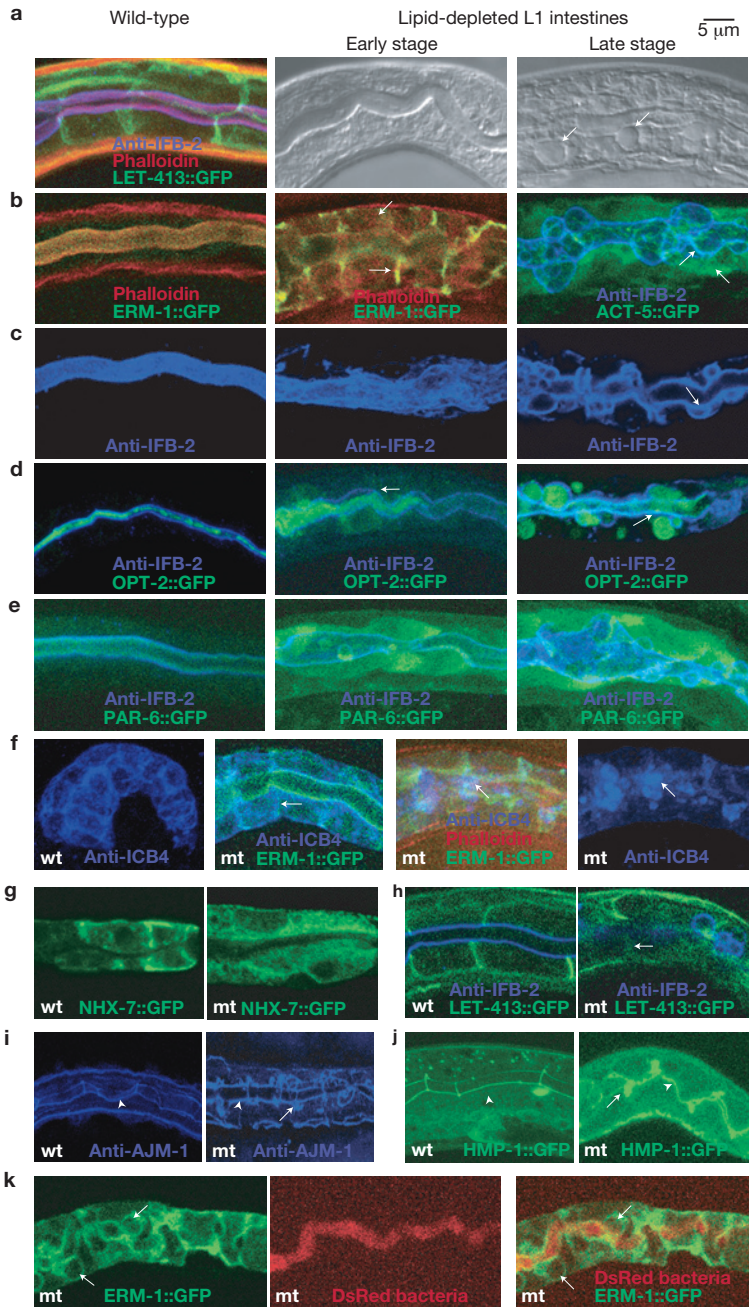

Figure 2 Apicobasolateral membrane and apical junction components in lipid-biosynthetic-enzyme-depleted intestines. (Supplementary Fig. S4 shows additional components.) (**a**–**e**) Apical membrane. (**a**) Left to right: confocal microscopy image of actin (phalloidin) overlay (purple) with intermediate filaments (IFB-2) at apical, and LET-413 at basolateral, membranes; Nomarski images: early phenotype lacks visible changes, later stage shows lateral lumens (arrows). (**b**) Left to right: apical actin/ERM-1 overlay (yellow); displaced basolaterally (yellow, lower arrow) and cytoplasmically (red, upper arrow); cortical actin (ACT-5)/IFB-2 overlay displaced to lateralized lumenal membranes (turquoise, left arrow) and cytoplasm (green, right arrow). (**c**) Left to right: apical submembraneous IFB-2; unravelling from lumen; displaced to lateralized lumenal membranes (arrow indicates central-lumenal IFB-2 contiguity). (**d**) Left to right: OPT-2, a transmembraneous oligopeptide transporter, positioned apical to IFB-2 (green without overlay); displaced basolaterally (arrow); displaced lateral to lateralized IFB-2 (green without overlay; note displacement to, but not expansion into, the lateral domain (arrow)). (**e**) Left to right: IFB2/PAR-6 overlay (turquoise); cytoplasmic PAR-6 displacement at early and late stage (green). (**f**–**h**) Basolateral membrane. (**f**) Left to right: ICB4 stains an unknown panmembraneous marker in wild type (wt); apicobasolateral ERM-1/ICB4 overlay (turquoise, arrow) in early-stage mutant (RNAi) phenotype (mt); ICB4 subapical accumulation (blue, arrow) in late-stage mutant; same image with separated ICB4 for clarity. (**g**) NHX-7, a basolateral integral membrane Na^+/H^+ pump, retained at basolateral membranes, but partially cytoplasmically displaced in late-stage mutant. (**h**) Basolateral LET-413, a junction-mediated polarity determinant[59], excluded from apical membrane in wild type (no IFB2 overlap) and also from lateralized ectopic lumenal membrane in mutant, but not displaced from the basolateral membrane (arrow). (**i**,**j**) Apical junctions. The junction integrity molecule AJM-1 and the adherens junction component HMP-1 remain contiguous at apicolateral boundaries in both wild type and mutant (arrowheads), but additionally surround nascent lateral lumens in mutant (arrows; note absence of fragmented junction pattern). (**k**) Feeding of dsRed-labelled bacteria fails to label ectopic lumens (arrows) or the cytoplasm of mt (same sections in all). Confocal images of representative L1 intestinal sections are shown: *pod-2-, let-767-, acs-1-* and *sptl*-1 RNAi cause the same mislocalization/localization of all markers ($N > 40$ for each marker).

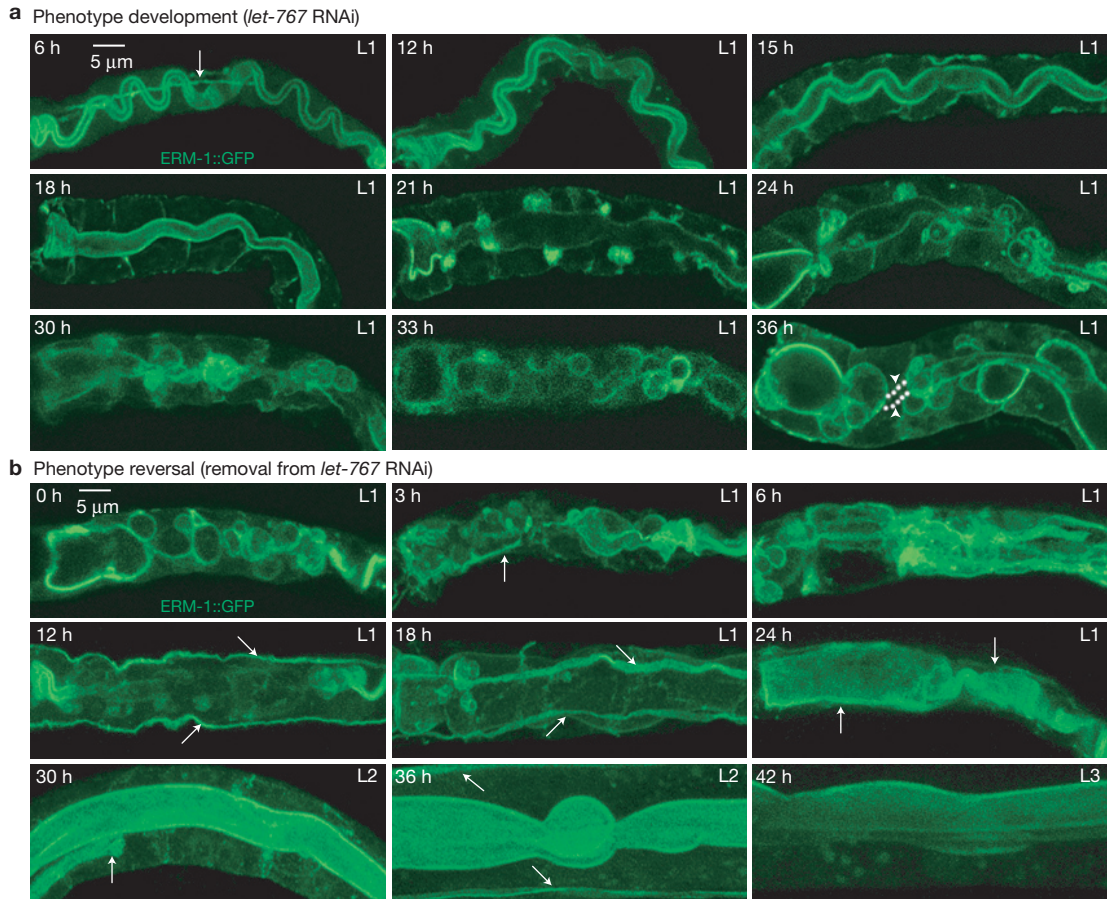

Figure 3 Lipid biosynthesis perturbations reversibly shift apicobasal domain identities and lumen position on expanding intestinal membranes *in situ*. (**a**) Tracking ERM-1::GFP displacement/placement after lipid-biosynthesis inhibition (0 h, hatching of *let-767(RNAi)* progeny, not shown): 6 h, apical (excretory canal visible in this image, arrow); 12 h, as puncta in cytoplasm; 15 h, as puncta at basal membranes; 18 h, entire basolateral membranes outlined; 21 h, enriched at apicolateral angle and disappearing from apical membrane; 24 h, at lateral lumens in apicolateral angle; 30 h, at multiple ectopic lumens along lateral membranes; 33 h, at enlarging ectopic lumens; 36h, at separate lateral lumens, almost lost from original apical membrane (arrowheads bracket central lumen area, dotted line indicates missing apical ERM-1::GFP). (**b**) Tracking ERM-1::GFP replacement/placement subsequent to lipid biosynthesis restoration (0 h, removal from *let-767* RNAi): 0 h, at multiple lateral lumens; 3 h, at smaller lateral lumens; 6 h, at lateral lumens and cytoplasmic; 12 h, cytoplasmic (blurred outlines of small lateral lumens still visible); 18 h, fully cytoplasmic, reappearing at widened contiguous apical membrane (hidden behind excretory canal, arrows); 24 h, at the centring apical/lumenal membrane, lateral lumens no longer visible; 30 h, at the wide central apical membrane and lateral membranes, now without lumens; 36 h, at the fully restored although undulating apical membrane; 42 h, at the apical membrane in the extended epithelium. The 42 h image encompasses 2 INT rings whereas the 0 h image includes all 9 INT rings: difference reflects epithelial expansion (note stage progression to L2 (30 h) and L3 (42 h); compare with L1 arrest 36 h post-RNAi induction (**a**)). Representative animals are shown, $N > 200$; confocal sections or projections on the level of the intestine: full projections in **b** to encompass all ERM-1::GFP; arrows indicate superimposed excretory canals.

-polarity-complex component PAR-6. Basolateral molecules, including the polarity determinant LET-413 (the Scribble homologue), were less affected, although partially displaced subapically (Fig. 2a–h and Supplementary Fig. S3a–d). Transmission electron microscopy (TEM) revealed corresponding structural conversions of apical and basolateral domains: microvilli and the submembraneous terminal web were lost apically and acquired laterally, identifying lateral openings as true lumens rather than membrane adhesion defects or intracellular vacuoles (Fig. 1c,d and Supplementary Figs S1c and S3h).

Apicobasal polarity defects of developing epithelia have been characterized as polarity loss through membrane equilibration and as unilateral, typically apical, domain expansion; both changes generally caused by apical junction defects[3,7]. In contrast, we find polarity conversion: apical characteristics are coincidentally lost from the original apical, and gained by the original lateral domain. In further contrast, intestines lacked typical apical junction defects[20]: loss, fragmentation or displacement of AJM-1, HMP-1 (the α-catenin homologue) and DLG-1 (the Discs-large homologue) from apicolateral junctures; ultrastructural defects at apicolateral sealing positions; and label uptake from fluorescently labelled bacterial food into intercellular spaces. Conversely, after polarity conversion but before single lateral lumen formation, additional junctions formed between nascent lateral lumens, indicating that they may contribute to *de novo* apical domain biogenesis on the lateral side rather than reflecting an assembly defect preceding and causing the polarity alteration (Figs 1c and 2i–k and Supplementary Fig. S3e–h).

We conclude that interference with any one of four distinct lipid-biosynthetic enzymes converts intestinal apicobasal membrane domain identities, generating separate lateral lumens.

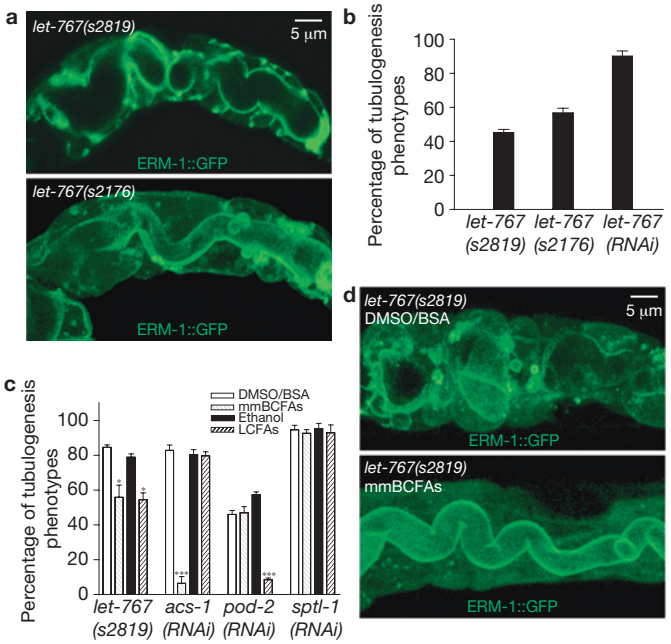

Figure 4 Germline mutations in fatty-acid-biosynthetic enzymes cause intestinal tubulogenesis defects that are rescued with exogenous fatty acids. An allelic series of *let-767* point mutations[26] includes: *s2176*, suggested null (early larval lethality); *s2819*, moderately severe (mid-larval lethality); and *s2464*, less severe allele (reaches adulthood with lethal progeny (maternal-effect)). (**a**) Top, confocal image of *s2819* with early basolateral ERM-1::GFP displacement; bottom, *s2176* with early ectopic lumen formation (*let-767(s2167/s2819) dpy-17(e164) unc-32(e189)III; sDp3(III;f); fgEx13(perm-1::erm-1::gfp rol-6(su1006))*). Lateral ERM-1::GFP displacement and ectopic lumen formation are obscured in the Dpy background with widened intestinal lumen and body shape. (**b**) Penetrance and expressivity of tubulogenesis defects (speed of development and number and size of lateral lumens) increase with allelic severity. Higher penetrance by RNAi than in *s2176* indicates maternal product requirement. All animals were evaluated 30 h post-hatching. Mean ± s.d. shown, $n = 5$ ($N > 200$ animals per experiment) for mutants and $n = 5$ ($N > 1{,}000$ animals per experiment) for RNAi animals. (**c**) Rescue with exogenous lipids supplied by food. mmBCFAs partially rescue *let-767-*, fully rescue *acs-1-*, but not *pod-2(RNAi)* tubulogenesis defects; straight-chain LCFAs partially rescue *let-767-*, fully rescue *pod-2-*, but not *acs-1(RNAi)*. *sptl-1(RNAi)* defects are not rescued with either mmBCFAs or straight-chain LCFAs. Experimental and control animals were evaluated 60 h post-feeding with fatty acids/solvents (Methods). Mean ± s.d. is shown, $n = 5$ ($N > 200$ animals per experiment), $^{*}P < 0.05$ and $^{***}P < 0.001$, two-tailed *t*-test. (**d**) Top, moderately severe *let-767(s2819)* allele (later stage of phenotype development than in **a**); bottom, almost fully rescued with exogenous mmBCFAs.

Lipid-biosynthetic enzymes affect apical sorting during *de novo* membrane biogenesis

C. elegans intestinal cell division, migration and intercalation are complete at mid-embryogenesis. To determine whether the late-embryonic or larval polarity changes reflected a role of lipid-biosynthetic enzymes in polarity maintenance rather than establishment, enzymes were RNAi-inactivated post-embryogenesis (Methods). This was sufficient to displace ERM-1::GFP basolaterally and switch lumen position in the mature larval, but not adult, epithelium (Supplementary Fig. S4a). Lipid-biosynthetic enzymes thus maintain post-mitotic intestinal polarity, but only in larvae, not in adults (a potential early embryonic requirement, for example through maternal lipids, cannot be excluded).

The morphogenetic feature distinguishing larval from adult intestines is net growth[21], indicating that the polarity function of lipid-biosynthetic enzymes may be linked to epithelial expansion. Consistent with this, full polarity conversion, although confined to one stage (the arrest stage, late embryo or L1), required an extended period of time where animals grow (~two days at 20 °C; Fig. 3a). Notably, growth suppression through food deprivation[22] attenuated it, indicating that membrane expansion was required to manifest the polarity change (Supplementary Fig. S4b,c). To explore the role of lipid-biosynthetic enzymes in *de novo* polarized membrane biogenesis, we searched for a newly apically delivered polarized molecule that was laterally displaced on lipid-biosynthesis perturbations. ERM-1::GFP recovery after *erm-1(RNAi)* removal revealed that ERM-1 is continuously supplied to larval, but not adult, lumenal membranes (peak delivery in L1 larvae; Supplementary Fig. S5). As ERM-1::GFP is displaced from expanding, but not non-expanding (starved) larval or adult membranes, these enzymes must target new components to the apical membrane during its biogenesis.

If lipid-biosynthetic enzymes maintain polarity by sorting newly synthesized membrane components, the effect of their loss might be reversible. To investigate this, their activity was restored in enzyme-depleted RNAi larvae with ectopic lumens. Strikingly, lipid-biosynthesis reactivation reversed apical membrane lateralization, closed lateral lumens, rebuilt a contiguous central lumen and rescued growth-arrest and lethality (Fig. 3b and Supplementary Fig. S4b–d for comparison with Dauer-dependent arrest reversal).

We conclude that specific components of lipid biosynthesis are required to sort apical molecules during *de novo* membrane biogenesis, sustaining apicobasal domain identities and a contiguous lumen in *C. elegans* intestinal epithelia.

Polarized membrane biogenesis requires saturated long-chain-fatty-acid biosynthesis

We considered that *pod-2-*, *let-767-*, *acs-1-* and *sptl-1(RNAi)*-induced polarity defects might result from the loss of a common single lipid product, although these enzymes were not components of an obvious biosynthetic pathway. We first examined POD-2, LET-767 and ACS-1, all biochemically defined fatty-acid-biosynthetic enzymes with intestinal localization[23–25]. Knockdowns were validated as specific and severe losses-of-functions by confirming ERM-1::GFP displacement in *pod-2(ye60)* intestines[25] (not shown) and demonstrating increasing polarity and tubulogenesis defects in an allelic series of *let-767* loss-of-function mutants[26] (Fig. 4a,b).

Disrupting biosynthetic pathways increases upstream substrates while decreasing downstream products. It was thus unlikely that toxic intermediates would induce polarity defects generated by losing different enzymes, including one catalysing the first committed step in *de novo* lipid biosynthesis (POD-2). Confirming this, exogenous fatty acids rescued the phenotype, in addition to the previously demonstrated wild-type gene rescue[23,25] (Fig. 4c,d). This result also excluded non-lipid-related dual enzyme functions and supported the assumption that losing one or more lipid compounds generated the phenotype.

Next, we knocked down 162 genes known or predicted to contribute to fatty-acid biosynthesis, metabolism or transport. Animals were examined for tubular polarity defects and negative results were

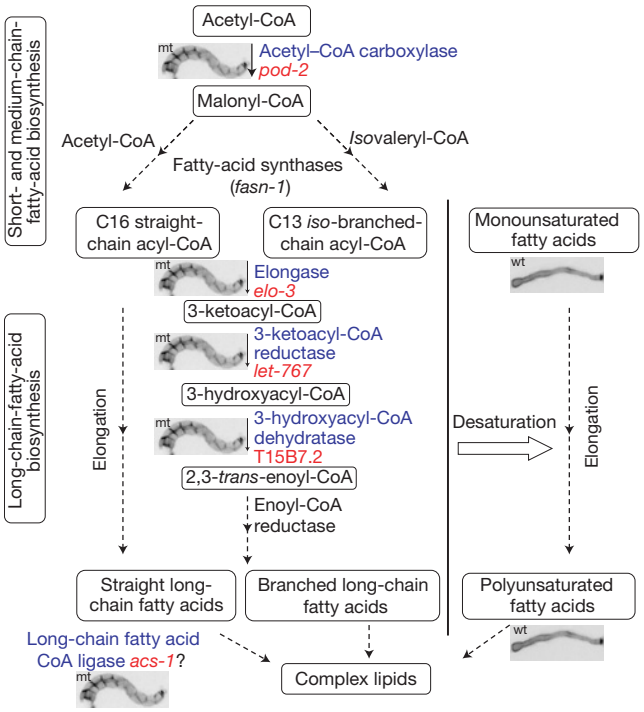

Figure 5 Tubular polarity requires saturated LCFA biosynthesis. Conserved fatty-acid-biosynthesis pathways are shown[56]. POD-2 and FASN-1 catalyse the first steps in saturated small- and medium-chain-fatty-acid biosynthesis (top: acetyl–CoA shown as primer example for even-numbered SFAs, *iso*valeryl-CoA for odd-numbered mmBCFAs), subsequently elongated to LCFAs by elongases (middle: this area was probed in greater detail and has been expanded; see text), variably desaturated by desaturases (right). All products are precursors for complex lipids (bottom). The presence or absence of polarity defects (wild-type (wt) or mutant (mt) indicated throughout by image insets) was evaluated in RNAi animals and/or germline mutants (see Supplementary Table S1 for specific genes targeted ($N = 162$), most of which lacked polarity defects; see Supplementary Fig. S6 for phenotypes). Identified enzymes are shown in blue, and corresponding genes are shown in red. *fasn-1(RNAi)* was not identified here because of its early arrest (*pod-2* and *fasn-1* are the only lipid-biosynthetic enzymes previously shown to affect polarity, at the first-cell stage; the mediating lipid compound was not identified[25]). The precise pathway location of *acs-1* is not known. Decreasing cholesterol levels to trace amounts did not produce the phenotype (not shown; *C. elegans* is a cholesterol auxotroph, but requires such low amounts of cholesterol that its role as a structural membrane lipid has been questioned[60]).

confirmed in selected germline mutants at pathway branch points (Fig. 5 and Supplementary Table S1). One additional enzyme was identified: ELO-3, an elongase predicted to generate LCFAs (Fig. 5 and Supplementary Fig. S6a). The identification of ELO-3 supported those of POD-2, LET-767 and ACS-1, with POD-2 catalysing the first step synthesizing short- and medium-length saturated fatty acids (SFAs; LCFA building blocks) and the others directly contributing to LCFA biosynthesis of straight or monomethyl branched-chain fatty acids[23,24,27] (mmBCFAs).

As elongases condense fatty acids to ketoacyl-CoA, we reasoned that ELO-3 might generate the substrate for the 3-ketoacyl-CoA reductase LET-767. To examine the enzymatic step downstream of this reductase we searched the *C. elegans* genome for an orthologue predicted to use the LET-767 product 3-hydroxy-acyl-CoA as a substrate and identified 3-hydroxyacyl-CoA dehydratase homology in the PTP-like protein T15B7.2. Its knockdown copied the phenotype (Fig. 5 and Supplementary Fig. S6b), indicating that ELO-3, LET-767 and T15B7.2 catalyse consecutive steps in the biosynthesis of the presumed polarity-affecting lipid.

In contrast, desaturase gene knockdowns did not generate the polarity defect. Desaturases synthesize mono- and polyunsaturated fatty acids[28,29] (MUFAs and PUFAs). This negative result was confirmed in the non-redundant strong loss-of-function allele *fat-2(wa17)* that lacks normal PUFAs (ref. 29; Fig. 5, not shown), although not additionally confirmed in germline mutants of redundant MUFA desaturases[28].

We conclude that a putative common lipid species should contain saturated LCFAs, possibly MUFAs, probably mmBCFAs, but not PUFAs, excluding many lipid-signalling molecules and phosphoinositides as candidates for this specific polarity function.

Saturated LCFA biosynthesis determines polarity through sphingolipid synthesis

We next examined the fourth identified enzyme, SPTL-1, predicted to condense a fatty acid with serine to form the long-chain-base (LCB) sphinganine as the first committed step in *de novo* sphingolipid synthesis (Figs 6a and 7a). As expected, fatty acids did not rescue its RNAi phenotype (Fig. 4c). The role of sphingolipid in polarity was, however, confirmed through *sptl-1(RNAi)* phenocopy by: double knockdowns of *sptl-2* and *sptl-3*, two additional *C. elegans* SPTs (Supplementary Fig. S6e); and feeding myriocin or fumonisin B, mycotoxins specifically inhibiting SPT and ceramide synthase, respectively. Both inhibitors dose-dependently induced the phenotype (Fig. 7a and Supplementary Fig. S6c). As ceramide synthase generates ceramide from sphinganine, we infer that sphinganine itself, previously suggested to affect polarity in hepatoma cell lines[30], is excluded here because both sphinganine loss (through myriocin and *sptl-1(RNAi)*) and excess (through fumonisin) generate the phenotype.

Ceramide (Cer), the building block of all complex sphingolipids, contains a second LCFA in addition to the one used for the LCB (Fig. 6a). Sphingolipid synthesis is thus strictly dependent on LCFAs, generally SFAs, and, in *C. elegans*, mmBCFAs (ref. 31), but not PUFAs, making sphingolipids good candidates for the putative common lipid compound. A series of experiments supported this idea. First, *pod-2-*, *acs-1-* and *let-767(RNAi)* phenotypes failed to efficiently reverse when sphingolipid synthesis was inhibited (Fig. 6b). Second, mild *sptl-1-*, *pod-2-* and *acs-1(RNAi)* enhanced moderate *let-767* alleles (not shown) and were themselves dominantly enhanced by *let-767(s2819);sDp3* (Fig. 6c). Third, mass spectrometry profiles of selected sphingolipids showed similar decreases in *let-767-*, *acs-1-* and *sptl-1(RNAi)* animals (Fig. 6d,e and Supplementary Table S3). These profiles also confirmed that *C. elegans* sphingolipids use C17 mmBCFAs for the LCB (ref. 31), and demonstrated that saturated LCFAs are used for the ceramide. Finally, exogenous sphingolipids partially rescued the polarity phenotype of animals deficient for fatty-acid-biosynthetic enzymes (see below).

We conclude that *pod-2, let-767, acs-1*, *elo-3* and T15B7.2 are *C. elegans* sphingolipid-biosynthesis pathway components, and as such they are required for tubular polarity. We also note that the essential but unknown mmBCFA function[27] at least partially results from it contributing to polarity and tubulogenesis through sphingolipid synthesis.

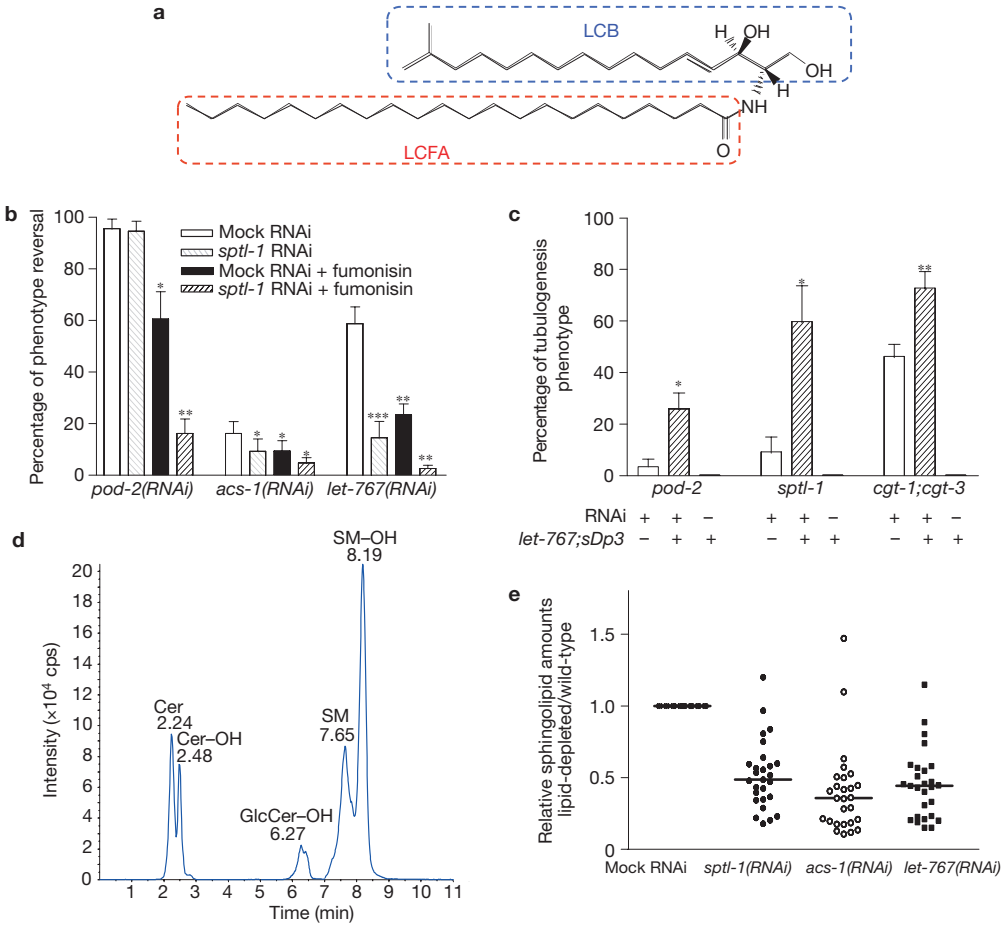

Figure 6 Fatty-acid biosynthesis determines tubular polarity through sphingolipid synthesis. (**a**) Ceramide: the sphingoid base (LCB) is linked to an LCFA through an amide bond (22:0 hydroxy-15 methyl-2-aminohexadec-4-en-1, 3-diol is shown). (**b**) Reversal of polarity conversion, induced by fatty-acid-biosynthetic-enzyme depletion, requires sphingolipid synthesis. Note, fumonisin (with and without *sptl-1* RNAi), but not *sptl-1(RNAi)* alone (or myriocin, not shown), suppresses *pod-2(RNAi)* polarity reversal. Thus, POD-2 uses LCBs generated during its suppression, indicating that it predominantly generates ceramide LCFAs. Conversely, *acs-1*- and *let-767(RNAi)* polarity reversal is suppressed by *sptl-1* alone, indicating that they lack such LCBs and thus contribute to their synthesis. This is consistent with the role of *let-767* and *acs-1* in mmBCFA synthesis, and the role of *pod-2* and *let-767* in straight LCFA synthesis[23–25] (the LCB requires mmBCFAs; ref. 31) and with the rescue experiments shown in Fig. 4b. Conditions of sphingolipid biosynthesis reduction were titrated to prevent induction of the phenotype on their own (Methods; under these conditions, *sptl-1(RNAi)* is enhanced by fumonisin). For comparison, identical RNAi conditions were used throughout: different reversal efficiencies thus reflect phenotype severity (varies with each enzyme, see Supplementary Figs S1 and S6; for example, standard *acs-1* RNAi induces a strong phenotype, less easily reversed). Mean ± s.d. is shown, $n = 4$ ($N > 60$ animals per experiment) $^{*}P < 0.05$, $^{**}P < 0.01$ and $^{***}P < 0.001$, two-tailed *t*-test. (**c**) Dominant genetic interactions between fatty-acid and sphingolipid-biosynthetic enzymes. *let-767(s2819);sDp3* are wild type; thus, any increase of polarity defects it induces in RNAi animals demonstrates enhancement. *pod-2* and *sptl-1* RNAi were titrated to generate no phenotypes, *cgt-1;cgt-3(RNAi)* was induced at standard conditions. Mean ± s.d. is shown, $n = 5$ ($N > 300$ animals per experiment), $^{*}P < 0.05$, $^{**}P < 0.01$, two-tailed *t*-test. (**d**) Ion chromatogram of wild-type worm extracts shown for the [M+H]+ *m/z* 250.3u fragment of their common d17:1 sphingoid base. Interpretation of mass ions from mass spectra of each peak: 2.24 min:d17:1ceramides (Cer), 2.48 min:d17:1hydroxyceramides (Cer–OH), 6.27 min:d17:1glucosylhydroxyceramides (GlcCer–OH), 7.65 min:d17:1sphingomyelins (SM), 8.19 min:d17:1 hydroxysphingomyelins (SM–OH). Here and below: synchronized wild-type or enriched RNAi L1 larvae were collected from ~800 plates each (Methods). (**e**) Decreased sphingolipid levels in both sphingolipid- and fatty-acid-biosynthesis-depleted animals. Relative amounts are plotted (C21-26–Cer, –Cer–OH, -GlcCer–OH, C21–23,25-SM and –SM–OH; Supplementary Table S3). Bars indicate median; wild type arbitrarily set at 1; dots represent individual compounds. Concentrations calculated from the mass-spectrometry-derived response ratio of compound area/internal standard area of the corresponding period per sample dry weight.

Polarity depends on ceramide glucosyltransferases

To identify the putative common polarity-affecting sphingolipid species, we knocked down 85 genes predicted to contribute to complex lipid and sphingolipid metabolism and regulation, adding double and triple RNAi and RNAi-sensitive conditions to detect redundant enzymes and mild effects (Fig. 7a and Supplementary Table S2, Methods). The phenotype was found in the single knockdown of a predicted sphingolipid fatty-acid hydroxylase, C25A1.5, and the double knockdown of the CGT orthologues *cgt-1* and *cgt-3* (Supplementary Fig. S6d,f). CGTs generate only glucosylceramide (GlcCer), the GSL backbone[17], and, in contrast to the previously identified enzymes, do not produce substrates for the biosynthesis of multiple lipids. This result therefore identifies GSLs as the furthest downstream polarity-affecting lipid species, and indicates that their loss generates the polarity defects induced by its ten upstream lipid-biosynthetic enzymes.

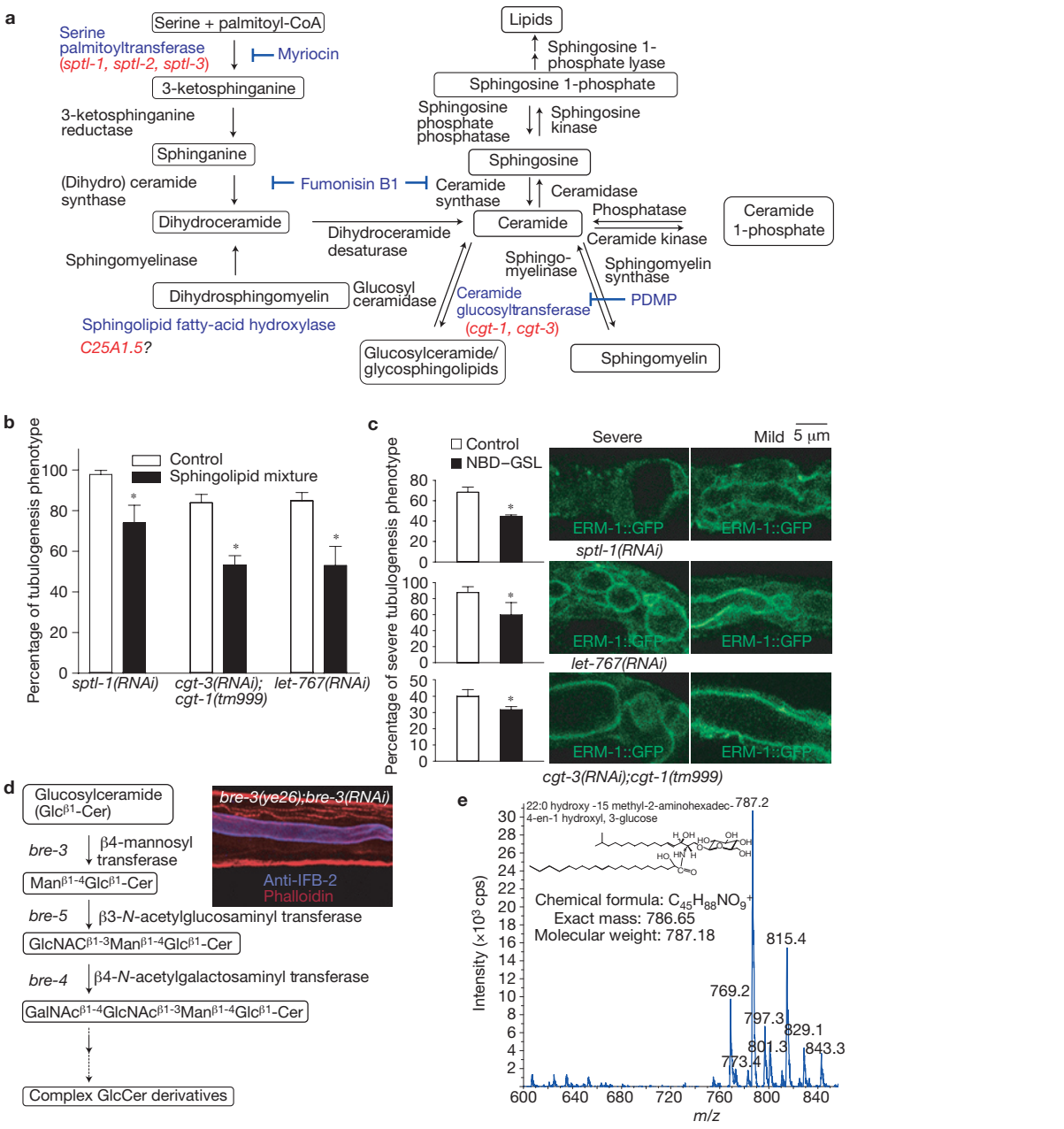

Figure 7 Tubular polarity requires CGTs and GSLs. (**a**) Conserved sphingolipid metabolic pathways are shown[56]. Left, *de novo* biosynthesis; right, salvage pathway; bottom, complex membrane sphingolipid biosynthesis. Presence/absence of polarity defects were assessed in RNAi animals and/or germline mutants (see Supplementary Table S2 for specific genes targeted ($N = 85$), most of which lacked polarity defects; see Supplementary Fig. S6 for phenotypes). Identified enzymes are shown in blue, and corresponding genes are shown in red. The precise location of sphingolipid fatty-acid hydroxylase is unknown. (**b**) *sptl-1-*, *cgt-1(tm999);cgt-3-* and *let-767(RNAi)* tubulogenesis defects are partially rescued by exogenous sphingolipids. A sphingolipid standard mixture, containing ten different sphingolipid compounds, was fed with RNAi bacteria (Methods). The percentage of animals with tubulogenesis defects was evaluated 64–66 h after feeding with lipids or solvents (control). Mean ± s.d. is shown, $n = 5$ ($N > 200$ animals per experiment), $^*P < 0.05$, two-tailed *t*-test. (**c**) NBD–C6-GlcCer (NBD–GSL) supplementation attenuates ectopic lumen formation in *sptl-1-*, *let-767-* and *cgt-1(tm999);cgt-3-(RNAi)* L1 intestines. Animals were evaluated for 'severe' (discontinuous central lumen/large ectopic lumens) versus 'mild' (partially contiguous central lumen/small ectopic lumens) phenotypes 5 and 6 days after feeding with GSLs or solvents (control; supplied with RNAi bacteria). For *sptl-1* RNAi, which induces the strongest phenotype, 'severe' was defined as arrest/intestinal disintegration and 'mild' as mobile/intestine not disintegrated. Confocal microscopy sections of representative animals are shown. Mean ± s.d., $n = 5$ ($N > 200$ animals per experiment), $^*P < 0.05$, two-tailed *t*-test. (**d**) The arthro-series of GlcCer derivatives is dispensable for the function of GlcCer in tubular polarity. The first steps of insect-type GlcCer-derivative biosynthesis are shown, and corresponding *C. elegans* orthologues are on the left[39]. The inset demonstrates intact intestinal lumen (purple) in the presumed null allele *bre-3(ye28)* combined with *bre-3(RNAi)* (animals grow to fertile adults)[39]. $N > 2,000$. (**e**) Accumulated mass spectra of wild-type GlcCer–OH with an elution peak of 6.27 min (Fig. 6d). GlcCer with *m/z* 787.2, with a C17 sphingoid base and a hydroxylated saturated C22 fatty-acid chain, was present in greatest abundance (inset). Hydroxyacylamines with saturated C21 (*m/z* 773.4) and C23-26 carbon chains (*m/z* 801.3, 815.4, 829.1, and 843.3, respectively) were present in low abundance. Peak *m/z* 769.2 may represent [M-4H] C21:0-d17:1 and peak *m/z* 797.3 may represent [M-4H] C23:0-d17:1 GlcCer–OH compounds.

Several findings further supported the role of CGTs and GSLs in tubular polarity. Previous studies determined that: *C. elegans* CGTs are expressed and function cell-autonomously in the intestine; they synthesize GSLs *in vitro* and *in vivo*; and arrested *cgt-1,ctg-3*-double and *cgt-1,ctg-2,ctg*-3-triple RNAi/mutant larvae have decreased although not absent GSL levels[32–35]. We found the polarity phenotype in double *cgt-1(tm999);cgt-3(tm504)* mutants, different combinations of *cgt-1,cgt-3*-double mutant/RNAi animals and in animals fed with the CGT inhibitor D,L-threo-PDMP (Supplementary Fig. S6f,g, not shown; Methods). Although complex membrane lipids may not be expected to recapitulate their endogenous roles as end products on membranes[36] (in contrast, exogenous fatty acids can function as metabolic intermediates or signalling molecules[24,25]; compare Fig. 4c,d), exogenous labelled and unlabelled sphingolipids were tested for rescue. Neither we nor others could rescue *cgt-1;cgt-3*-double-mutant/RNAi-induced lethality with exogenous GSLs (ref. 34); however, feeding a mixture of synthetic sphingolipids (including GSLs), made to human templates, mildly improved *ctg-1(tm999);ctg-3(RNAi)* tubulogenesis defects, and NBD–C6-GlcCer uptake attenuated their severity (Fig. 7b,c).

Without excluding other possible sphingolipid contributions, additional results indicated that GSLs mediate the polarity effect of their upstream fatty-acid- and sphingolipid-biosynthetic enzymes: moderate *cgt-;cgt-3(RNAi)* polarity phenotypes were dominantly enhanced by *let-767(s2819);sDp3* (Fig. 6c); *ctg-1(tm999);ctg-(RNAi)*-rescuing sphingolipids and GSLs likewise partially rescued *let-767(RNAi)* and *sptl-1(RNAi)* tubulogenesis defects that were similarly attenuated by NBD–C6-GlcCer (Fig. 7b,c); mass spectrometry profiles showed comparable GSL losses in fatty-acid- and sphingolipid-biosynthesis-defective animals (Supplementary Fig. S7a and Table S3). Of note, the complex membrane sphingolipids GSL and sphingomyelin ratio was consistently altered, with a greater loss of GSLs, indicating a corresponding change in membrane lipid composition (Supplementary Fig. S7b).

We conclude that the furthest downstream lipid-biosynthetic pathway enzyme CGT, and its product GlcCer, are required for tubular polarity, indicating that GSLs are the polarity-affecting common lipid species.

Polarity requires hydroxylated GlcCer, whereas further sugar modifications are dispensable

GSLs could affect polarity through GlcCer intermediates, derivatives or GlcCer itself. The systematic approach of the pathway screen largely excludes the first: gaining and losing multiple different intermediates of eleven GSL-biosynthetic enzymes equally disturbs polarity. This includes ceramide, the immediate metabolite of GlcCer (single and double RNAi of glucocerebrosidases also failed to generate the phenotype, although multiple-null mutants were not tested; Supplementary Table S2). As GSL metabolism occurs on endomembranes[37], it cannot, however, be excluded that they function through an organelle-sequestered intermediate subfraction.

Further sugar modifications of the GlcCer backbone create the large GSL family[38]. Single knockdowns of 112 gene candidates for the biosynthesis or function of GlcCer derivatives (Supplementary Table S4), including those previously ordered into a biosynthetic pathway for insect-specific derivatives[39], failed to generate the polarity phenotype. *bre-3(ye26)*, a viable, presumed null allele for a β4-mannosyltransferase that catalyses the first step in their biosynthesis, confirmed these negative results, excluding the arthro-series of GlcCer-derivatives as required for this function (Fig. 7d).

Our mass spectrometry profile furthermore revealed the complete absence of lactosylceramide and consequently the entire GSL lacto-series (Supplementary Fig. S7c,d), supporting previous assumptions that *C. elegans*, similarly to *Drosophila*, exclusively uses the arthro-series of GlcCer derivatives[39,40]. In the absence of as-yet-unidentified GSL sugar modifications, these results indicate that GlcCer itself exerts the polarity effect, for which additional sugar modifications are dispensable.

Finally, our mass spectrometry analysis characterized GlcCer as invariably hydroxylated, consistent with the identified sphingolipid fatty-acid hydroxylase, C25A1.5, and containing a saturated LCFA of C21–C26 chain length, with C22 in greatest abundance (Fig. 7e).

We conclude that the polarity-affecting lipid compound is probably GlcCer–OH itself, with or without specific sugar modifications, with a C17 branched-chain LCB and a saturated LCFA of length C21–C26, probably C22 (Fig. 7e, inset).

GSL biosynthesis affects vesicular trafficking

GSLs localize to endothelial vesicle membranes and lumenal plasma membranes, are synthesized on vesicle membranes and apically sort several membrane molecules in mammalian epithelial cell lines[8,14,41]. Feeding partially rescuing BODIPY–C5-Cer and NBD–C6-GlcCer indicated that both lipids also localize to vesicles and the lumenal membrane of the *C. elegans* intestine (Fig. 8a).

Consistent with a conserved GSL trafficking function were the following findings: low-temperature interference with trafficking suppressed the polarity conversion, indicating that vesicular transport was required to reveal the misdirection of apical membrane components (Fig. 8b and Supplementary Fig. S8a–g; note, low temperature also slows growth and development); *sptl-1(RNAi)* intestinal sections revealed vesicle paucity, along with distended endoplasmic reticular and Golgi membranes (Fig. 8c and Supplementary Fig. S8h,i); the *pod-2-*, *let-767-*, *acs-1-*, *sptl-1(RNAi)* and *cgt-1(tm999)/cgt-3(RNAi)*-induced polarity conversion depleted intestinal endosomes, primarily RAB-11-associated, presumed lumenal-membrane-forming vesicles[4,42] (Fig. 8d, not shown). RAB-11-positive vesicles were first slightly enlarged, then lost from the apical membrane; RAB-5-associated early endosomes were occasionally mildly enlarged subapically; L1-specific RAB-7-positive apical clusters, but not the presumed Golgi-associated mid-cytoplasmic endosomes, were decreased in number or absent; RAB-10-associated basolateral recycling endosomes were least affected[43]. α-mannosidase II (MANS) -associated Golgi membranes, distributed as mini-stacks throughout the wild-type *C. elegans* cytoplasm[43,44], contracted basolaterally, assuming a linear, possibly tubulated, pattern (Fig. 8d).

Finally, BODIPY–C5-Cer and NBD–C6-GlcCer, which only mildly improve polarity defects, were themselves displaced to lateral ectopic lumens in *sptl-1(RNAi)* and *cgt-1(tm999)/cgt-3(RNAi)* intestines (Fig. 8e), demonstrating that GSL biosynthesis also affects the targeting of lipids, including its own apical placement. Given the membrane association of GSLs, this finding further supports a function of GSL biosynthesis in the vesicular delivery of apically destined molecules during membrane biogenesis.

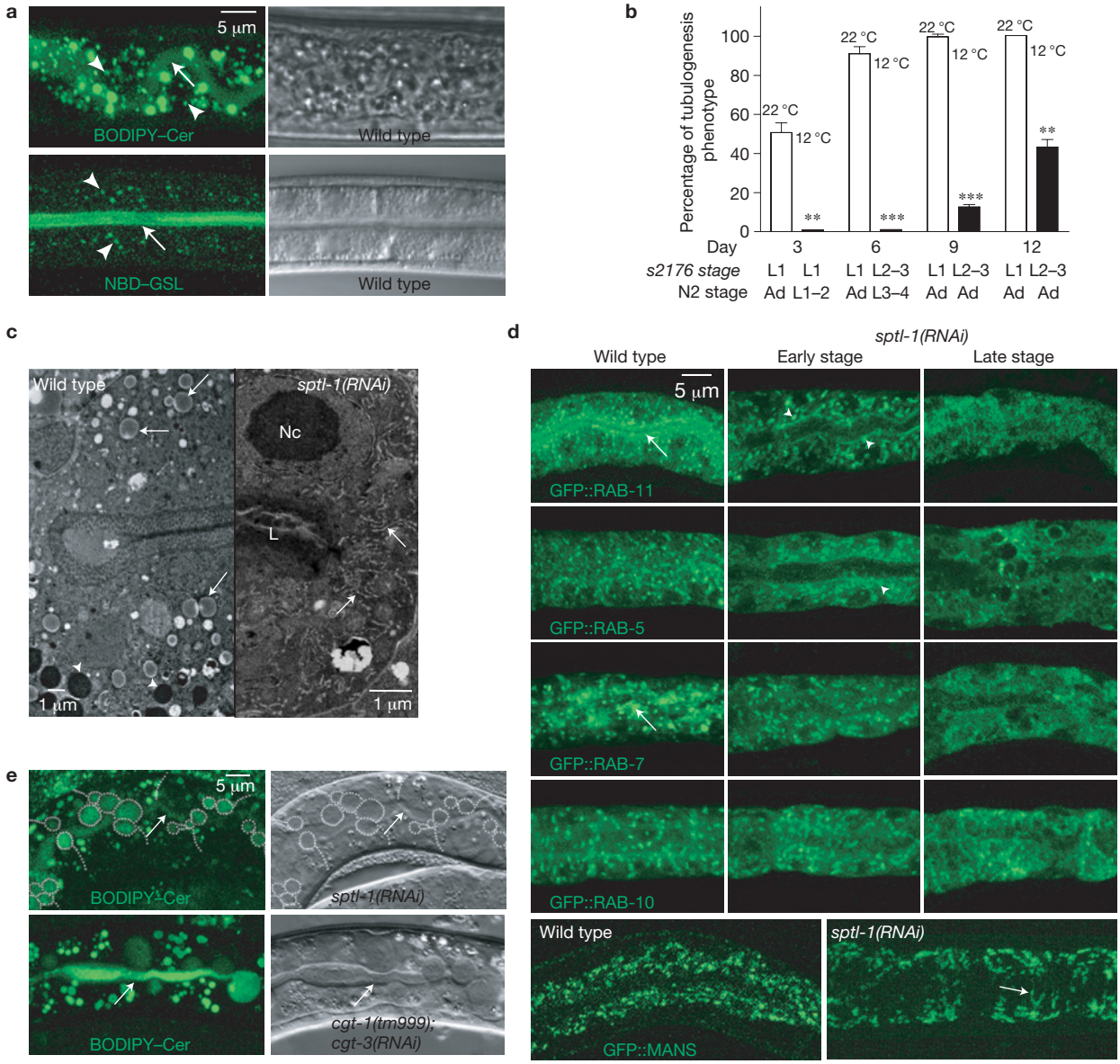

Figure 8 Subcellular localization of exogenous sphingolipids and the effects of sphingolipid-biosynthesis suppression on vesicular trafficking. (**a**) BODIPY–C5-Cer (top) and NBD–C6-GlcCer (NBD–GSL, bottom), supplied with food, localize to intestinal vesicles (arrowheads) and apical/lumenal plasma membranes (arrows) of wild-type animals. Over time, both exogenous lipids accumulate in larger vesicles (NBD–GSL-fed animal is shown immediately after lipid supplementation; Methods). Lumenal membrane lipids are distinguishable from intra-lumenal lipids in NBD–GSL-fed animal. Left, confocal microscopy images; right, corresponding Nomarski images. (**b**) Low-temperature interference with trafficking[61,62] inhibits polarity conversion (compare Supplementary Fig. S8). At 12 °C, the *let-767(s2176)* typical moderate polarity defects are suppressed and animals progress beyond L1 arrest to L2/L3. Developmental stages (larval: L1—4, adult: Ad) at 12 and 22 °C on days 3, 6, 9 and 12 post-bleaching are shown beneath the bars (Methods). Mean ± s.d. shown, $n = 4$ ($N > 120$ animals per experiment) $^{**}P < 0.01$, $^{***}P < 0.001$, two-tailed t-test. (**c**) TEM L1 intestinal cross-sections (Supplementary Fig. S8 shows whole intestines): vesicle abundance and variety in wild type (left; including lipid-storage vesicles (arrows) and yolk vesicles (arrowheads)); vesicle paucity and profusion of distended endoplasmic reticular and Golgi membranes (arrow shows example) in *sptl-1(RNAi)* (right; note lumen deformation and missing apical microvilli). L, lumen; Nc, nucleus. (**d**) Apical endosome populations become depleted during polarity conversion. Left to right, progression to late-stage polarity defect (representative L1 intestines shown): lumenal-membrane-associated RAB-11 (arrow) is lost; pancytoplasmic RAB-11-positive vesicles are first mildly enlarged (arrowheads), then mostly lost. Pancytoplasmic RAB-5-positive vesicles are more slowly and less severely depleted (arrowhead indicates occasionally enlarged subapical vesicles). L1-specific subapical RAB-7-positive vesicle aggregates (arrow) are lost; the pancytoplasmic fraction is unchanged or moderately decreased. Pancytoplasmic RAB-10-positive vesicles are moderately decreased in number. The evenly dispersed vesicular MANS-positive Golgi stacks (GFP::MANS) aggregate basolaterally in linear rather than vesicular structures (arrow; compare text). (**e**) BODIPY–C5-Cer displacement to ectopic lateral lumenal membranes in *sptl-1(RNAi)*- (top) and *cgt-1(tm999)/cgt-3(RNAi)* L1 intestines (bottom; confocal images left, corresponding Nomarski images right). Cer-positive ectopic lumenal membranes show lateral membrane connections (outlined by dots (top)) and are distinct from cytoplasmic vesicles; arrows indicate main lumen. All confocal images in this figure are collected at settings limiting autofluorescent vesicle interference.

DISCUSSION

The long-proposed essential role of GSLs in development has remained mysterious, and their postulated contribution to *in vivo* polarity uncertain[14,19,45,46]. Here, an unbiased genetic tubulogenesis screen uncovers an essential role for GSLs in maintaining polarity and a central lumen in the developing *C. elegans* intestine. Our analysis indicates that endo- and plasma-membrane-associated GSLs determine polarity by sorting new components to expanding apical membranes: their loss simultaneously decreases molecular and structural apical characteristics at original apical membranes while increasing them at original lateral membranes; this polarity conversion diverts newly synthesized membrane components from their apical path; it requires cell growth and trafficking, but not cell division, migration or junction disassembly; it is reversible in single cells on restoration of lipid biosynthesis; it depletes apical endosomes, including RAB-11-associated lumenal vesicles; and it affects the presumed membrane-associated apical delivery of GSLs themselves. Without excluding additional GSL roles in structural membrane biogenesis or other trafficking aspects, an apical sorting function is strongly supported by the documented ability of GSLs to apically deliver several molecules in mammalian cell lines[8,11,12,15]. Our findings in turn now provide evidence for the relevance of these *in vitro* findings for polarized tissue morphogenesis *in vivo*, and for the proposition that GSLs may determine apical plasma membrane domain identity[47]. GSLs, similarly to phosphoinositides, may combine aspects of both endo- and plasma-membrane-based polarity cues, suggesting a mode of integration for these distinct membrane-associated polarity determinants[2]. Phosphoinositides, classical vesicle-based sorting signals[9], do, in fact, control plasma membrane domain identity and affect mammalian tubulogenesis *in vitro*[5,48,49].

Previously characterized core polarity determinants of developing epithelia, such as the Par-, Crumbs- and Scribble-related protein complexes, were characterized in proliferating and migrating cells or cell populations[2,3,7]. Our *in vivo* single-cell analysis of post-mitotic expanding epithelia, which separated membrane biogenesis from proliferation- and migration-dependent polarity cues, may have allowed the identification of the innate sorting ability of these structural membrane lipids during *de novo* membrane biogenesis. This analysis also revealed unanticipated aspects of polarity and tissue plasticity: polarity remains dynamic in single post-mitotic cells; the lumen position is flexible in a fully constructed tube epithelium; and both polarity and lumen position can be reversibly shifted on the growing membrane *in situ* by lipid-biosynthesis modulation.

The sorting function of GSLs in mammalian cell lines was linked to the formation of rafts, thought to form on lumenal vesicle- and plasma-membrane leaflets[10,50,51]. However, GlcCer, the GSL backbone without sugar modification, is uniquely placed on cytoplasmic membrane leaflets, a location distinct from its derivatives and of unknown significance[14]. Here it may directly interact with apically destined cytoplasmic molecules, polarity determinants or coat complexes. Intriguingly, loss of *tat-2*, the gene encoding a *C. elegans* flippase that vertically translocates lipids between membrane leaflets, rescues the lethality of *sptl-1* and mmBCFA loss[52]. If TAT-2 were to flip GlcCer to the lumenal leaflet, its loss would increase GlcCer at the cytoplasmic leaflet where it could improve apical transport. A GSL-specific flippase was postulated, but has not yet been identified[14,17].

Whereas GlcCer sugar modifications are deemed critical for sorting in mammalian cell lines[8] (a finding so far not confirmed by targeted deletions of the genes encoding their biosynthetic enzymes in mice[19]), we found them dispensable for tubular polarity *in vivo*. The vertebrate- and invertebrate-specific lacto- and arthro-series of GlcCer-derivatives can be swapped in *Drosophila* for developmental functions[53], indicating tolerance for sugar modifications, emphasizing the importance of the sphingolipid backbone, and further supporting its interspecies conserved function. In intriguing agreement with our findings, epithelial polarization in mammalian cell lines was recently linked to GSL glycans[54], and to an sphingomyelin- to GSL-biosynthesis switch, with an increase in GSL fatty-acid length, saturation and hydroxylation[55].

GlcCer (or GlcCer–OH), as part of complex GSLs, may also affect sorting through lipid–lipid-microdomain or lipid–protein-shell formation on lumenal membrane leaflets[18,50,51]. Our finding that GSL biosynthesis positions the apical domain during *de novo* membrane biogenesis is unexpectedly consistent with the original, but subsequently abandoned, proposition that GSLs segregate the apical plasma membrane through endomembrane maturation during bulk membrane biogenesis[16]. The dose-dependent effect of GSLs on polarity and the rescue of moderate GSL-dependent polarity defects by growth restriction indicate that the relative proportions of GSLs may be critical for polarized membrane biogenesis. The dependency of the apical placement of GSLs on their own biosynthesis is consistent with a requirement for their endomembrane-associated synthesis, a scenario compatible with the proposed polarizing component of membrane biogenesis by lipid-based self-organization[16].

Despite known functions in polarized morphogenesis *in vitro*[48,49], lipids escaped identification in numerous genetic polarity screens. Lipid-biosynthetic enzymes identified in genetic screens are often not pursued because they typically synthesize multiple compounds. Here we show that systematic biosynthetic pathway targeting, combined with genetic interaction studies, can identify an end-point biosynthetic enzyme, and thus a lipid species. Along with defining biosynthesis pathways (here, the *C. elegans* sphingolipid biosynthesis pathway), this approach can identify multiple proteins directly controlling a function of interest (here, eleven lipid-biosynthetic enzymes directly regulating tubular polarity), and may reveal functions of intermediates (here, the role of the enigmatic mmBCFAs in tubular polarity). Notably, the simultaneous generation of multiple loss- and gain-of-function conditions for downstream products and upstream substrates, respectively, inherent to this approach, helps distinguish primary from secondary changes, a particular conundrum of lipid analysis where intermediates are interconverted and compensatory changes frequent[56]. The additional biosynthetic screen for sugar modifications demonstrated that an identified lipid species can be further defined as a chemical compound and indicates that such screens can also be used for the analysis of sugars. This approach should be generally applicable to extend the power of unbiased genetic screens to non-proteinaceous compounds, identifying their *in vivo* cellular roles beyond known metabolic functions. □

METHODS

Methods and any associated references are available in the online version of the paper at http://www.nature.com/naturecellbiology

Note: Supplementary Information is available on the Nature Cell Biology website

ACKNOWLEDGEMENTS

Strains and plasmids were provided by D. Baillie (Fraser University, Burnaby, British Columbia, Canada), A. Croce (IFOM Istituto FIRC di Oncologia Molecolare, Milan, Italy), B. Grant (Rutgers University, Piscataway, New Jersey, USA), K. Kemphues (Cornell University, Ithaca, New York, USA), K. Nehrke (University of Rochester Medical Center, Rochester New York, USA), G. Ruvkun (Massachusetts General Hospital, Harvard Medical School, Boston, Massachusetts, USA), K. Strange (Vanderbilt University Medical Center, Salisbury Cove Maine, USA), J. Simske (Case Western Reserve University School of Medicine, Cleveland, Ohio, USA), S. Mitani (National Bioresource Project Japan) and the Caenorhabditis Genetics Center (NIH Center for Research Resources). We thank G. Ruvkun for the lethal RNAi library, and J. Moore (Avanti Polar Lipids); Mary McKee (MGH Microscopy Core/partially funded by the IBD grant DK43351 and BA DE award DK57521) and K. Nygen; Christopher Crocker; and Edward Membreno for contributions to LC/MS; TEM; illustrations and *C. elegans* maintenance, respectively. We thank F. Solomon and B. Winckler for critical reading of the manuscript and H. Weinstein and A. Walker for ongoing support. This work was supported by NIH grants HD044589 and GM078653 and a Mattina R. Proctor Award to V.G.

AUTHOR CONTRIBUTIONS

H.Z. generated and assembled most of the data and contributed to project design, data analysis and writing of the manuscript. N.A. participated in most experiments, carried out the glycosylation screen and contributed to experimental design and data analysis. L.A.K. contributed to the genetic interaction experiments. D.H.H. and J.T.F. contributed to electron microscopy experiments and J.T.F. to writing of the manuscript. V.G. conceived and directed the project, participated in experiments and wrote the manuscript.

COMPETING FINANCIAL INTERESTS

The authors declare no competing financial interests.

Published online at http://www.nature.com/naturecellbiology
Reprints and permissions information is available online at http://www.nature.com/reprints

1. Pfeffer, S. R. & Rothman, J. E. Biosynthetic protein transport and sorting by the endoplasmic reticulum and Golgi. *Annu. Rev. Biochem.* **56,** 829–852 (1987).
2. Mellman, I. & Nelson, W. J. Coordinated protein sorting, targeting and distribution in polarized cells. *Nat. Rev. Mol. Cell Biol.* **9,** 833–845 (2008).
3. St Johnston, D. & Ahringer, J. Cell polarity in eggs and epithelia: parallels and diversity. *Cell* **141,** 757–774 (2010).
4. Bryant, D. M. *et al.* A molecular network for *de novo* generation of the apical surface and lumen. *Nat. Cell Biol.* **12,** 1035–1045 (2010).
5. Martin-Belmont, F. & Rodriguez-Foretell, A. E. Acquisition of membrane polarity in epithelial tube formation patterns, signalling pathways, molecular mechanisms, and disease. *Int. Rev. Cell Mol. Biol.* **274,** 129–182 (2009).
6. Kemphues, K. J., Press, J. R., Morton, D. G. & Chang, N. S. Identification of genes required for cytoplasmic localization in early *C. elegans* embryos. *Cell* **52,** 311–320 (1988).
7. Nelson, W. J. Adaptation of core mechanisms to generate cell polarity. *Nature* **422,** 766–774 (2003).
8. Rodriguez-Boolean, E., Kibitzer, G. & Müsch, A. Organisation of vesicular trafficking in epithelia. *Nat. Rev. Mol. Cell Biol.* **6,** 233–247 (2005).
9. Di Paolo, G. & De Camilla, P. Phosphoinositides in cell regulation and membrane dynamics. *Nature* **443,** 651–657 (2006).
10. Lippincott-Schwartz, J. & Phair, R. D. Lipids and cholesterol as regulators of traffic in the endomembrane system. *Annu. Rev. Biophys.* **39,** 559–578 (2010).
11. Mays, R. W. *et al.* Hierarchy of mechanisms involved in generating Na/K-ATPase polarity in MDCK epithelial cells. *J. Cell Biol.* **130,** 1105–1115 (1995).
12. Sprong, H. *et al.* Glycosphingolipids are required for sorting melanosomal proteins in the Golgi complex. *J. Cell Biol.* **155,** 369–380 (2001).
13. Hoekstra, D., Maier, O., van der Wouden, J. M., Slimane, T. A. & van Ijzendoorn, S. C. D. Membrane dynamics and cell polarity: the role of sphingolipids. *J. Lipid Res.* **44,** 869–877 (2003).
14. Degroote, S., Wolthoorn, J. & van Meer, G. The cell biology of glycosphingolipids. *Semin. Cell Dev. Biol.* **15,** 375–387 (2004).
15. Mayor, S. & Riezman, H. Sorting GPI-anchored proteins. *Nat. Rev. Mol. Cell Biol.* **5,** 110–120 (2004).
16. Simons, K. & van Meer, G. Lipid sorting in epithelial cells. *Biochemistry* **27,** 6197–6202 (1988).
17. van Meer, G., Voelker, D. R. & Feigenson, G. W. Membrane lipids: where they are and how they behave. *Nat. Rev. Mol. Cell Biol.* **9,** 112–124 (2008).
18. Lingwood, D. & Simons, K. Lipid rafts as a membrane-organizing principle. *Science* **327,** 46–50 (2010).
19. Furukawa, K., Tokuda, N., Okuda, T. & Tajima, O. Glycosphingolipids in engineered mice: insights into function. *Semin. Cell Dev. Biol.* **15,** 389–396 (2004).
20. Lynch, A. M. & Hardin, J. The assembly and maintenance of epithelial junctions in *C. elegans*. *Front. Biosci.* **14,** 1414–1432 (2009).
21. Knight, C. G., Patel, M. N., Azevedo, R. B. & Leroi, A. M. A novel mode of ecdysozoan growth in *Caenorhabditis elegans*. *Evol. Dev.* **4,** 16–27 (2002).
22. Baugh, L. R. & Sternberg, P. W. DAF-16/FOXO regulates transcription of cki-1/Cip/Kip and repression of lin-4 during *C. elegans* L1 arrest. *Curr. Biol.* **16,** 780–785 (2006).
23. Entchev, E. V. *et al.* LET-767 is required for the production of branched chain and long chain fatty acids in *Caenorhabditis elegans*. *J. Biol. Chem.* **283,** 17550–17560 (2008).
24. Kniazeva, M., Euler, T. & Han, M. A branched-chain fatty acid is involved in post-embryonic growth control in parallel to the insulin receptor pathway and its biosynthesis is feedback-regulated in *C. elegans*. *Genes Dev.* **22,** 2102–2110 (2008).
25. Rappleye, C. A., Tagawa, A., Le Bot, N., Ahringer, J. & Aroian, R. V. Involvement of fatty acid pathways and cortical interaction of the pronuclear complex in *Caenorhabditis elegans* embryonic polarity. *BMC Dev. Biol.* **3,** 8 (2003).
26. Kuervers, L. M., Jones, C. L., O'Neil, N. J. & Baillie, D. L. The sterol modifying enzyme LET-767 is essential for growth, reproduction and development in *Caenorhabditis elegans*. *Mil. Genet. Genomics* **270,** 121–131 (2003).
27. Kniazeva, M., Crawford, Q. T., Seiber, M., Wang, C. Y. & Han, M. Monomethyl branched-chain fatty acids play an essential role in *Caenorhabditis elegans* development. *PLoS Biol.* **2,** E257 (2004).
28. Brock, T. J., Browse, J. & Watts, J. L. Fatty acid desaturation and the regulation of adiposity in *Caenorhabditis elegans*. *Genetics* **176,** 865–875 (2007).
29. Watts, J. L. & Browse, J. Genetic dissection of polyunsaturated fatty acid synthesis in *Caenorhabditis elegans*. *Proc. Natl Acad. Sci. USA* **99,** 5854–5859 (2002).
30. Van Ijzendoorn, S. C. D., Van Der Wouden, J. M., Liebisch, G., Schmitz, G. & Hoekstra, D. Polarized membrane traffic and cell polarity development is dependent on dihydroceramide synthase-regulated sphinganine turnover. *Mol. Biol. Cell* **15,** 4115–4124 (2004).
31. Chitwood, D. J., Lusby, W. R., Thompson, M. J., Kochansky, J. P. & Howarth, O. W. The glycosylceramides of the nematode *Caenorhabditis elegans* contain an unusual, branched-chain sphingoid base. *Lipids* **30,** 567–573 (1995).
32. Ichikawa, S. & Hirabayashi, Y. Glucosylceramide synthase and glycosphingolipid synthesis. *Trends Cell Biol.* **8,** 198–202 (1998).
33. Leipelt, M. *et al.* Glucosylceramide synthases, a gene family responsible for the biosynthesis of glucosphingolipids in animals, plants, and fungi. *J. Biol. Chem.* **276,** 33621–33629 (2001).
34. Marza, E., Simonsen, K. T., Faergeman, N. J. & Lesa, G. M. Expression of ceramide glucosyltransferases, which are essential for glycosphingolipid synthesis, is only required in a small subset of *C. elegans* cells. *J. Cell Sci.* **122,** 822–833 (2009).
35. Nomura, K. H. *et al.* Ceramide glucosyltransferase of the nematode *Caenorhabditis elegans* is involved in oocyte formation and in early embryonic cell division. *Glycobiology* **21,** 834–848 (2011).
36. Maier, O., Oberle, V. & Hoekstra, D. Fluorescent lipid probes: some properties and applications (a review). *Chem. Phys. Lipids* **116,** 3–18 (2002).
37. Hannun, Y. A. & Obeid, L. M. Principles of bioactive lipid signalling: lessons from sphingolipids. *Nat. Rev. Mol. Cell Biol.* **9,** 139–150 (2008).
38. Varki, A. *Essentials of Glycobiology* 2nd edn (Cold Spring Harbor Laboratory Press, 2009).
39. Griffitts, J. S. *et al.* Glycolipids as receptors for *Bacillus thuringiensis* crystal toxin. *Science* **307,** 922–925 (2005).
40. Gerdt, S., Lochnit, G., Dennis, R. D. & Geyer, R. Isolation and structural analysis of three neutral glycosphingolipids from a mixed population of *Caenorhabditis elegans* (Nematoda:Rhabditida). *Glycobiology* **7,** 265–275 (1997).
41. Futerman, A. H. & Riezman, H. The ins and outs of sphingolipid synthesis. *Trends Cell Biol.* **15,** 312–318 (2005).
42. Weisz, O. A. & Rodriguez-Boolean, E. Apical trafficking in epithelial cells: signals, clusters and motors. *J. Cell Sci.* **122,** 4253–4266 (2009).
43. Chen, C. C. *et al.* RAB-10 is required for endocytic recycling in the *Caenorhabditis elegans* intestine. *Mol. Biol. Cell* **17,** 1286–1297 (2006).
44. Rolls, M. M., Hall, D. H., Victor, M., Stelzer, E. H. & Rapoport, T. A. Targeting of rough endoplasmic reticulum membrane proteins and ribosomes in invertebrate neurons. *Mol. Biol. Cell* **13,** 1778–1791 (2002).
45. Yamashita, T. *et al.* A vital role for glycosphingolipid synthesis during development and differentiation. *Proc. Natl Acad. Sci. USA* **96,** 9142–9147 (1999).
46. Rao, R. P. & Acharya, J. K. Sphingolipids and membrane biology as determined from genetic models. *Prostaglandins Other Lipid Mediat.* **85,** 1–16 (2008).
47. Schuck, S. & Simons, K. Polarized sorting in epithelial cells: raft clustering and the biogenesis of the apical membrane. *J. Cell Sci.* **117,** 5955–5964 (2004).
48. Gassama-Diagne, A. *et al.* Phosphatidylinositol-3,4,5-trisphosphate regulates the formation of the basolateral plasma membrane in epithelial cells. *Nat. Cell Biol.* **8,** 963–970 (2006).
49. Martin-Belmont, F. *et al.* PTEN-mediated apical segregation of phosphoinositides controls epithelial morphogenesis through Cdc42. *Cell* **128,** 383–397 (2007).
50. Haucke, V. & Di Paolo, G. Lipids and lipid modifications in the regulation of membrane traffic. *Curr. Opin. Cell Biol.* **19,** 426–435 (2007).
51. Simons, K. & Gerl, M. J. Revitalizing membrane rafts: new tools and insights. *Nat. Rev. Mol. Cell Biol.* **11,** 688–699 (2010).
52. Seamen, E., Blanchette, J. M. & Han, M. P-type ATPase TAT-2 negatively regulates monomethyl branched-chain fatty acid mediated function in post-embryonic growth and development in *C. elegans*. *PLoS Genet.* **5,** e1000589 (2009).

53. Wandall, H. H. *et al*. Egghead and brainiac are essential for glycosphingolipid biosynthesis *in vivo*. *J. Biol. Chem.* **280,** 4858–4863 (2005).
54. Mishra, R., Grzybek, M., Niki, T., Hirashima, M. & Simons, K. Galectin-9 trafficking regulates apical-basal polarity in Madin–Darby canine kidney epithelial cells. *Proc. Natl Acad. Sci. USA* **107,** 17633–17638 (2010).
55. Sampaio, J. L. *et al*. Membrane lipidome of an epithelial cell line. *Proc. Natl Acad. Sci. USA* **108,** 1903–1907 (2011).
56. Vance, D. E. & Vance, J. E. *Biochemistry of lipids, lipoproteins and membranes* 5th edn (Elsevier, 2008).
57. Gobel, V., Barrett, P. L., Hall, D. H. & Fleming, J. T. Lumen morphogenesis in *C. elegans* requires the membrane-cytoskeleton linker *erm-1*. *Dev. Cell* **6,** 865–873 (2004).
58. Sulston, J. E. & Horvitz, H. R. Post-embryonic cell lineages of the nematode, *Caenorhabditis elegans*. *Dev Biol.* **56,** 110–156 (1977).
59. Legouis, R. *et al*. LET-413 is a basolateral protein required for the assembly of adherens junctions in *Caenorhabditis elegans*. *Nat. Cell Biol*. **2,** 415–422 (2000).
60. Kurzchalia, T. V. & Ward, S. Why do worms need cholesterol? *Nat. Cell Biol*. **5,** 684–688 (2003).
61. Martinez-Alonso, E., Egea, G., Ballesta, J. & Martinez-Menarguez, J. A. Structure and dynamics of the Golgi complex at 15 °C: low temperature induces the formation of Golgi-derived tubules. *Traffic* **6,** 32–44 (2005).
62. Onelli, E., Prescianotto-Baschong, C., Caccianiga, M. & Moscatelli, A. Clathrin-dependent and independent endocytic pathways in tobacco protoplasts revealed by labelling with charged nanogold. *J. Exp. Bot.* **59,** 3051–3068 (2008).

nature cell biology

DOI: 10.1038/ncb2328

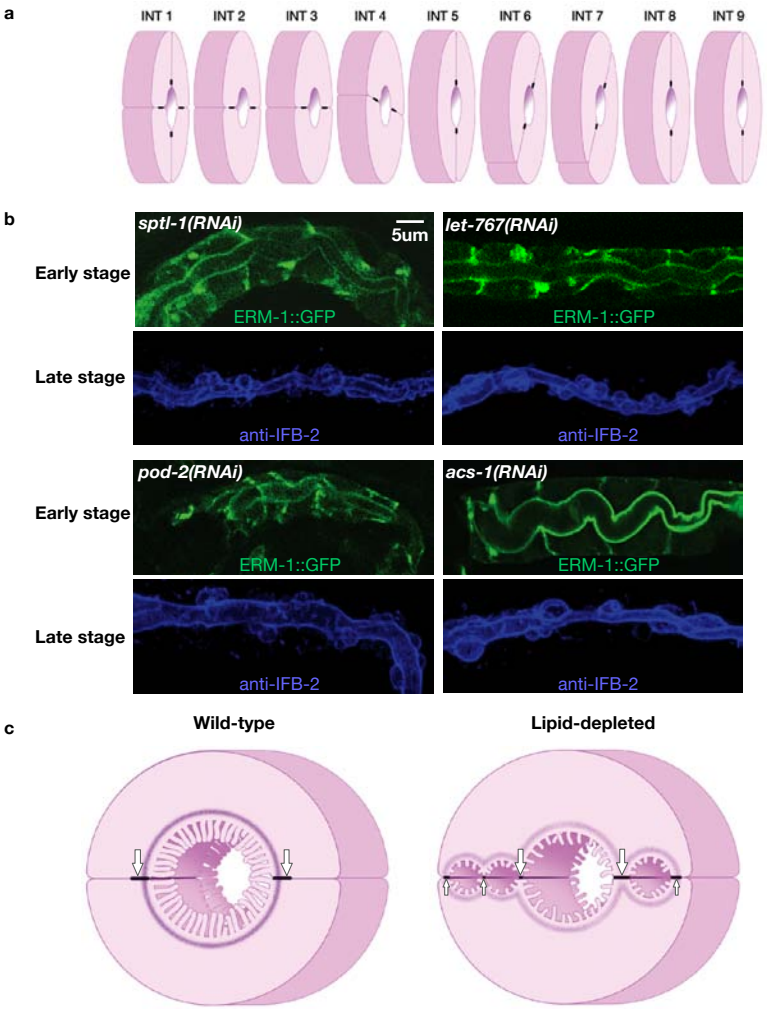

Figure S1 *C. elegans* intestinal morphogenesis and INT ring architecture in wild-type and lipid-biosynthetic-enzyme-deficient animals. **(a)** Schematic of the nine INT rings forming the mature wild-type intestine (compare to corresponding model and legend in Fig.1d; view here from posterior left lateral aspect). Apical junctions are shown, placed at apicolateral margins, surrounding and sealing the lumen between adjacent cells (black bars, compare Fig.1a). One electron dense unit covers both adherens- (apically placed) and tight/septate (basally placed) functional junction subunits[20]. After intercalation in mid-embryogenesis, no further cell division or migration occurs, but the epithelium expands during late embryogenesis and four larval stages (L1 – L4)[71]. Cell growth occurs continuously from the L1 stage onward, following a linear pattern during each larval stage that continues into the adult, assuming an exponential curve in molting larvae that flattens out in adults[21]. **(b)** Signature polarity/multiple lumen RNAi phenotype of the four lipid-biosynthetic enzymes identified in the global tubulogenesis screen. Here and below, initial basolateral ERM-1::GFP displacement is denoted as 'early stage' (top) and ectopic lumen formation as 'late stage' of phenotype development (bottom; this stage can be subdivided into an earlier stage of multiple small lateral lumens and a later stage of single large lateral lumens with central lumen discontinuity [compare Fig.1b/3a]). Lethality is >90% for all knockdowns at standard RNAi conditions (shown here, except for *pod-2*; Methods), with early larval lethality and a >90% penetrant tubulogenesis phenotype for *let-767-*, *acs-1-* and *sptl-1(RNAi)* (N>500). *pod-2(RNAi)* causes embryonic lethality with a lower penetrant tubulogenesis phenotype (~50%, phenotype development probably masked by the earlier lethality; Fig.S2). Milder *pod-2* RNAi conditions (shown here) phenocopy *let-767-*, *acs-1-* and *sptl-1(RNAi)*. Penetrance and expressivity depend on strength of interference and on the individual gene (standard RNAi conditions induce different phenotype severities in individual gene knockdowns [not shown]). **(c)** Higher magnification schematic of wild-type (left) and lipid-biosynthetic-enzyme depleted RNAi/mutant INT ring with ectopic lumens (right). Note reduced size and loss of microvilli and submembraneous terminal web (shown as ring below the lumenal membrane) from the central lumen with the concomitant emergence of both structures at ectopic lateral lumens in RNAi/mutant animal. Apicolaterally placed junctions remain intact at their wild-type location (large arrows), but additional lateral junctions form around ectopic lumens (small arrows). At a later stage of phenotype development, apical characteristics disappear from the central lumen, and larger lateral lumens form.

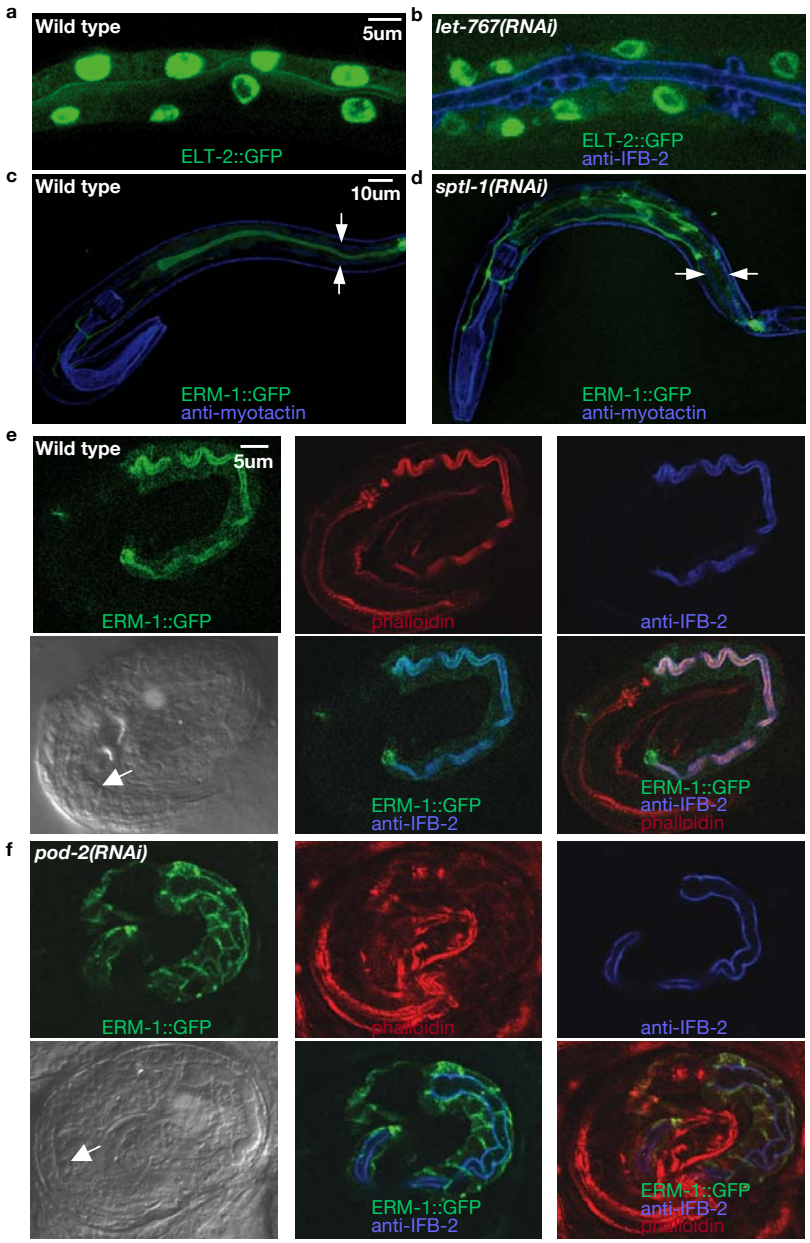

Figure S2 Lipid-biosynthetic-enzyme-deficient animals lack overall digestive tract morphogenesis defects or epithelial damage. **(a, b)** No change in number and morphology of nuclei (labeled with the intestinal transcription factor ELT-2) between lipid-biosynthetic-enzyme-deficient (b; IFB-2 outlines ectopic lumens) and wild-type intestines (a). **(c, d)** No obvious general digestive tract morphogenesis defects in lipid-biosynthetic-enzyme deficient animals (d), as compared to wild-type (c). Myotactin, labeling muscle basement membranes, outlines the shape of the digestive tract, including the pharynx and the external lining of the intestinal tube (arrows). ERM-1::GFP also labels the H-shaped excretory canals, in addition to intestinal apical membranes in wild-type (c) and lateral ectopic lumenal membranes in lipid-biosynthetic-enzyme-depleted animal (d). No intestinal proliferation or intercalation defects were found in any *pod-2-, let-767-, acs-1-* or *sptl-1(RNAi)* animals with full phenotype development (N>500). Confocal projections of L1 intestines are shown. **(e, f)** *pod-2(RNAi)* generates the polarity phenotype in the embryo. Confocal sections and Nomarski images of wild-type (e) and *pod-2(RNAi)* (f) 3-fold embryos: ERM-1::GFP, anti-IFB-2 and phalloidin (actin) colocalize at the apical membrane in wild-type (pink in e), while ERM-1 and actin are displaced to basolateral membranes in *pod-2(RNAi)* animals (yellow in f; red: additional cytoplasmic actin displacement). An early stage of apical marker displacement is shown, at which time the submembraneous lumenal cytoskeleton, outlined by IFB-2 (not yet displaced), is still intact (compare to e). Apical marker displacement thus precedes structural membrane transformation rather than being caused by it. Also note the overall wild-type body plan and organ shapes (arrows point to anterior bulb of pharynx in Nomarski images). Development of the intestinal phenotype in the embryo reveals that it is not caused by starvation or dependent on contact with external food sources.

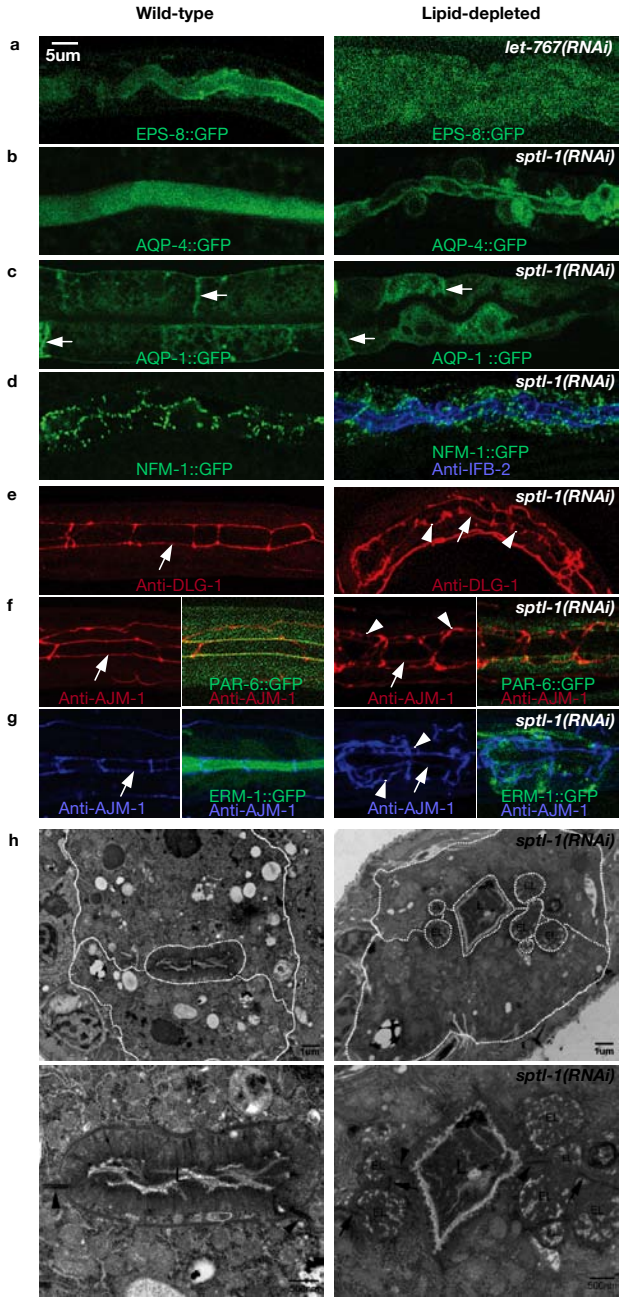

Figure S3 Placement of polarized membrane markers, junctions and structural domains in lipid-biosynthetic-enzyme-depleted intestines (compare to Fig.2). **(a)** The apical brushborder component human-epidermal-growth-factor-receptor-kinase-substrate-8 ortholog EPS-8[72] is cytoplasmically displaced in lipid-biosynthetic-enzyme-depleted intestines (increased laser power shown here to demonstrate loss of marker at apical membrane). **(b)** The apical membrane water channel AQP-4/Aquaporin[73] is displaced to ectopic lateral lumenal membranes in RNAi animals (confocal section shown here to demonstrate membraneous location around ectopic lumens). **(c)** The basolaterally enriched membrane water channel AQP-1/Aquaporin[73] (arrows) is mostly retained at basolateral membranes in RNAi animals. **(d)** The basolaterally enriched submembraneous ERM-1-family member NFM-1[57] retains its basolateral location in RNAi animals, but also collects in the sub-apical zone (an *nfm-1::gfp* construct with a punctate panmembraneous expression pattern is shown here). **(e)** The apical junction component DLG-1/Discs-Large[74] maintains its contiguous apical ladder pattern (arrows), but additionally surrounds lateral ectopic lumens in lipid-biosynthetic-enzyme-depleted animals (arrowheads). **(f - g)** The anti-AJM-1-labeled apical junction belt remains intact (arrows), although expanded around ectopic lumens (arrowheads), while apical PAR-6 is displaced to the cytoplasm (f) and ERM-1 (g) to lateral membranes and cytoplasm in RNAi animals. Confocal images of representative L1 intestines are shown in a - g (RNAi animals at stage of lateral lumen development; N>20). **(h)** TEM cross-sections of whole L1 intestines (top) with corresponding higher magnifications (bottom). Early ectopic lumen (EL) formation is shown, with multiple small lumens emerging along the lateral membrane in RNAi animal, surrounded by additional ectopic junctions that appear ultrastructurally normal. Large single lateral lumens arise at later stages of phenotype development, consistent with a possibly transient nature of these ectopic junctions (Fig.1b, lower right image). Serial sections in selected areas failed to reveal any ectopic lumens that were not either directly or indirectly (via other ectopic lumens) in contact with a lateral membrane. Intestinal plasma membranes are outlined for clarity; L, main apical lumen.

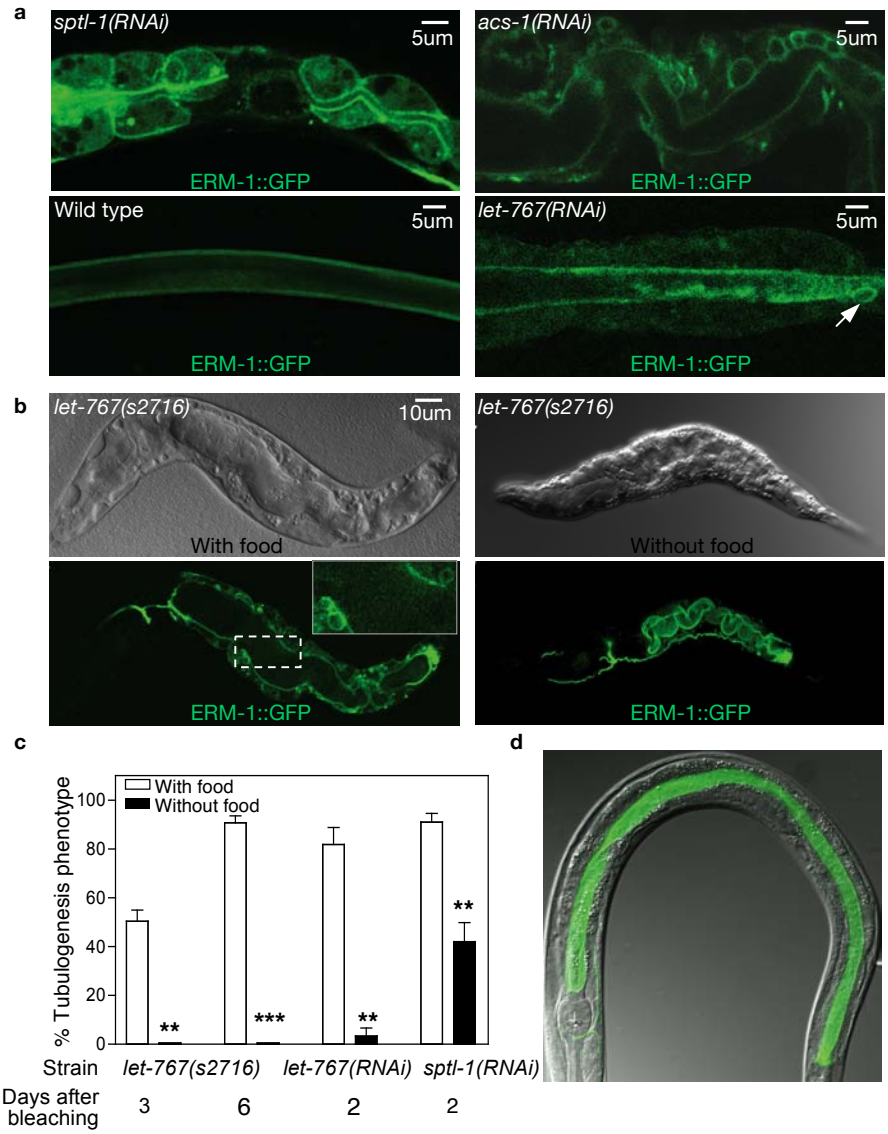

Figure S4 Polarity conversion and ectopic lumen formation can be induced on the expanding plasma membrane by interference with lipid biosynthesis. **(a)** Conditional RNAi with lipid-biosynthetic enzymes, induced after hatching (Methods), is sufficient to induce polarity conversion and ectopic lumen formation in larval, but not in adult, intestines. Basolateral ERM-1::GFP displacement in *sptl-1(RNAi)* L1 (upper left, *sptl-1* RNAi performed in an *rrf-3*-RNAi-sensitive background); ectopic lumen formation in *acs-1(RNAi)* L4 larva (upper right). A younger (day 5) wild-type adult (lower left) and an older (day 12) adult-induced *let-767(RNAi)* animal (lower right) are shown: an occasional apical membrane bleb (arrow) was noted in older animals, but no polarity or tubulogenesis defects (note: minimal cellular growth continues in adult animals[21]). N>50 for each gene. Single-section confocal images of typical animals are shown. **(b)** Starvation suppresses polarity conversion and ectopic lumen formation in lipid-biosynthetic-enzyme-depleted animals. Nomarski images (top) and corresponding confocal images (bottom) of *let-767(s2167)* mutants grown with (left) and without (right) food. Note the absence of ERM-1::GFP displacement and ectopic lumens in the bottom right panel. *let-767* mutants' Dpy background (left) obscures the fully developed, but only moderate, polarity and ectopic-lumen phenotype in food-supplied animals (magnified in inset; compare Fig.4). Note that non-starved *let-767* mutant L1s (left) are larger than starved L1s (right). Representative animals are shown, 3 days (left) and 6 days (right) after bleaching parents (corresponding to about 2 ½ and 5 ½ days after hatching, respectively). **(c)** The efficiency of phenotype suppression by starvation is inversely correlated with phenotype severity. *let-767(s2716)*, *let-767-* and *sptl-1(RNAi)* animals represent a series of animals with increasingly severe polarity defects (all arrest as L1/early larvae; compare Fig.4a,b, Fig. S1b). Moderate *let-767(s2716)* polarity defects are strongly suppressed, whereas severe *sptl-1(RNAi)* polarity defects are only partially suppressed by starvation (parental RNAi induction is sufficient for phenotype development). Mean +/- SD is shown, n=4 (N>150 animals per experiment), $^{**}P<0.01$, $^{***}P<0.001$, two-tailed *t* test. **(d)** Dauer larvae lack the polarity phenotype induced by interference with specific lipid-biosynthetic enzymes. Confocal/Nomarski overlay of Dauer larva with wild-type ERM-1::GFP placement and wild-type overall intestinal morphology. L2 Dauer or L1 diapause larvae[22, 75] share several characteristics with lipid-biosynthetic-enzyme-deficient larvae: they lack lipids; they arrest as early larvae; they are reversible upon nutrient (lipid) restoration; and Dauers have morphological changes of the digestive tract[75, 76]. Diapause-specific changes have also been reported for animals deficient in mmBCFAs and ELO-5[24, 27]. However, no dauer (N>500) or diapause animal exhibited obvious polarity defects (N>50; data not shown). L2/Dauers were collected from crowded starved plates, L1s were isolated by spotting bleached eggs on food-free NGM agar plates. Animals were observed daily for 3 weeks.

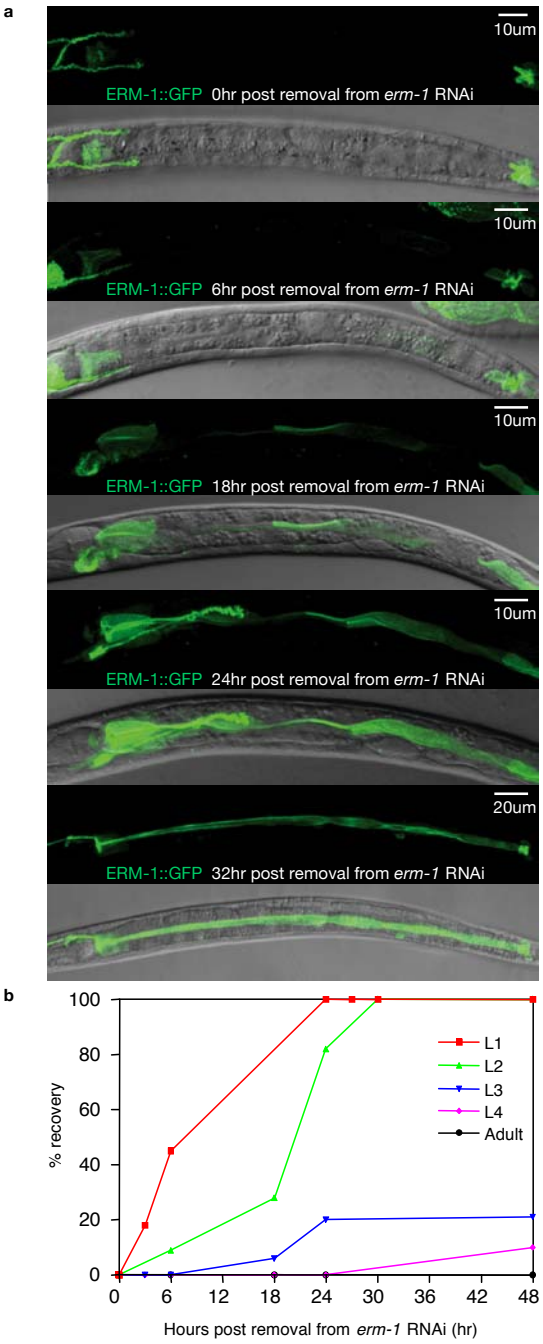

Figure S5 ERM-1::GFP recovery at the apical membrane of the postmitotic intestinal epithelium after its removal by *erm-1* RNAi. **(a)** Confocal images of intestines of ERM-1::GFP transgenic animals, with and without overlay of their corresponding Nomarski images, are shown. Conditions that eliminated ERM-1::GFP from the intestine without inducing L1 lethality were empirically determined. These conditions still show faint ERM-1::GFP at the anterior and posterior tips of the apical intestinal membrane, in the excretory canals and in the pharynx (top, left [anterior] and right [posterior] portions of the animal). *erm-1(RNAi)* L1, L2, L3, L4 larvae and adults lacking apical intestinal ERM-1::GFP were removed from *erm-1* RNAi bacteria at different time points, and observed for GFP recovery. Representative L1s (through 24hr) and L2s (32hr) are shown. Note the gradual recovery of ERM-1::GFP at the intestinal apical membrane during the expansion of the epithelium, while animals grow from L1- to L2-stage larvae. **(b)** Time course of ERM-1::GFP recovery at the apical membrane for different larval stages and adults (recovery was defined as ERM-1::GFP redelivery to more than 50% of the apical membrane). 96% (70/73) L1 and 90% (68/76) L2 recovered ERM-1::GFP completely by 24 hours and 30 hours, respectively, with L2s displaying uneven, albeit full staining of the apical intestinal membrane. 21% (14/67) L3 and 10% (6/61) L4 recovered fully and 69% (46/67) L3 and 84% (51/61) L4 recovered partially by 48 hours, suggesting that ERM-1 delivery to the apical membrane slows when the epithelium approaches full size (a low percentage [<10%] lethality among L3/4s suggests a mild contributing *erm-1[RNAi]* effect). In contrast, adult animals show no ERM-1::GFP recovery at the apical membrane at 48 hours although normal adults strongly express ERM-1::GFP at the apical membrane throughout their lifetime[57].

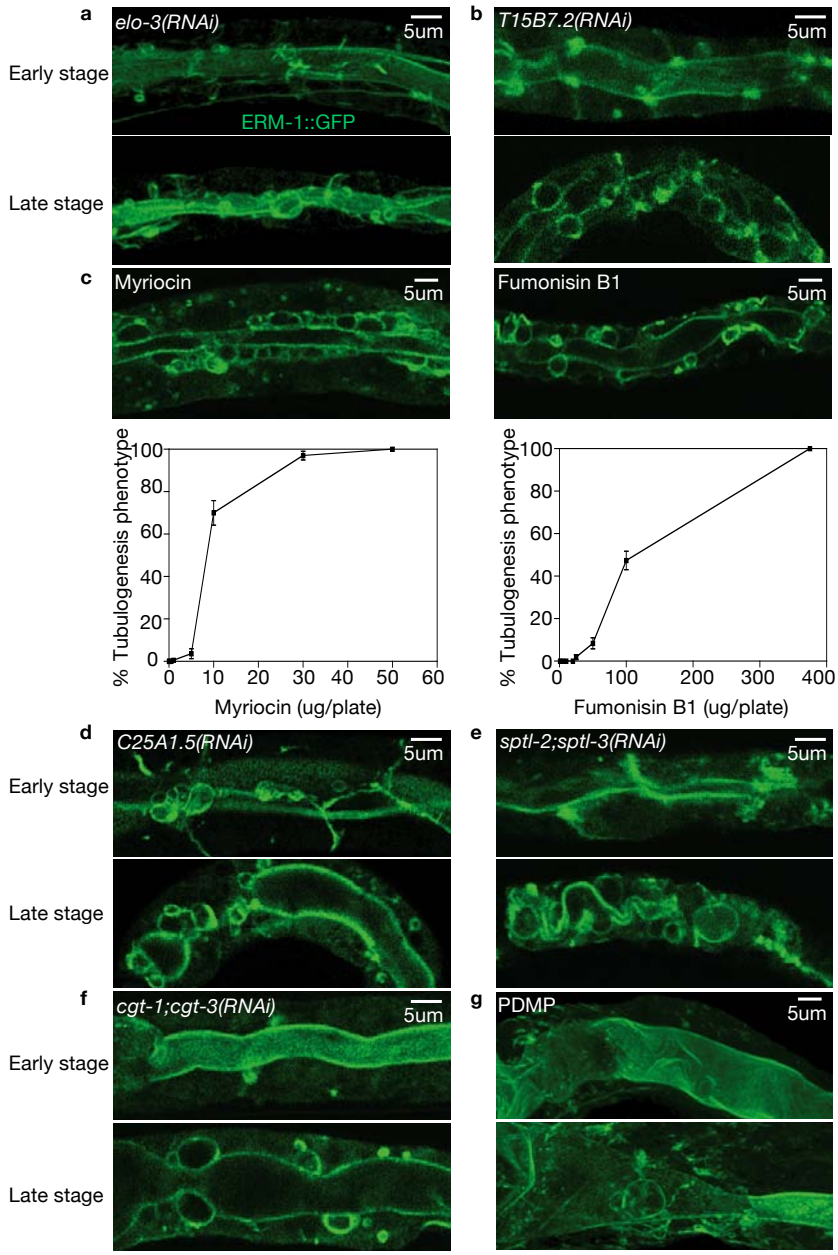

Figure S6 Targeted RNAi screens and enzyme inhibitors identify additional lipid-biosynthetic enzymes required for intestinal polarity and lumen position. Upper panels of each set (except c) show early basolateral ERM-1::GFP displacement, lower panels show subsequent ectopic lumen formation (confocal sections of L1-L3 larvae are shown). **(a, b)** *elo-3*: long chain fatty acid elongase (a) and *T15B7.2*: 3-hydroxyacyl-CoA dehydratase (b) are two additional fatty-acid-biosynthetic enzymes. **(c)** The sphingolipid-biosynthesis inhibitors Myriocin and Fumonisin B1 phenocopy the lipid-biosynthetic-enzyme-specific tubular polarity alteration. An L3 (Myriocin) and L1 (Fumonisin B1) animal with ectopic lumen formation are shown (Methods). Phenotype penetrance correlates with inhibitor concentration (bottom panels), consistent with its correlation with RNAi strength and allele severity in fatty-acid-biosynthetic-enzyme-depleted animals (Fig.4b). Note that the polarity phenotype was induced on the expanding membranes of animals hatched on mycotoxin containing plates (parents were grown on OP50). Between 105 and 245 animals were analyzed at each concentration of Myriocin and Fumonisin (mean +/- SD is shown, n=3). (**d - f**) *C25A1.5*: sphingolipid fatty acid hydroxylase (d), *sptl-2,-3*: serine palmitoyltransferases (e) and *cgt-1,-3*: ceramideglucosyltransferases (CGTs) (f) are additional sphingolipid-biosynthetic enzymes. *sptl-2,sptl-3* double RNAi was performed in an RNAi sensitive background (*rrf-3[pk1426]*). **(g)** The CGT inhibitor D,L-threo-PDMP but not C_4DGJ, C_9DGJ and C_4DNJ[77, 78] (not shown) induces a mild polarity phenotype in anterior INTs on the expanding membrane of developing larvae (parents grown on OP50). Penetrance and expressivity of both mutant and RNAi phenotypes vary among different biosynthetic enzymes and do not increase with their proximity to the furthest downstream enzyme (CGT) in the GSL-biosynthetic pathway (not shown). Note that lipid-biosynthetic-enzyme germline deletions and RNAis may result in various degrees of lipid compound depletion (GSLs are not even completely abolished in triple *cgt-1,-2,-3* mutant/RNAi animals[34]). Differences in enzyme kinetics may also contribute: for instance, interference with the upstream, but expected to be rate-limiting, enzymes POD-2 and SPTL-1 generates a severe phenotype, while interference with the furthest downstream enzyme pair CTG-1, -3 generates a less severe phenotype.

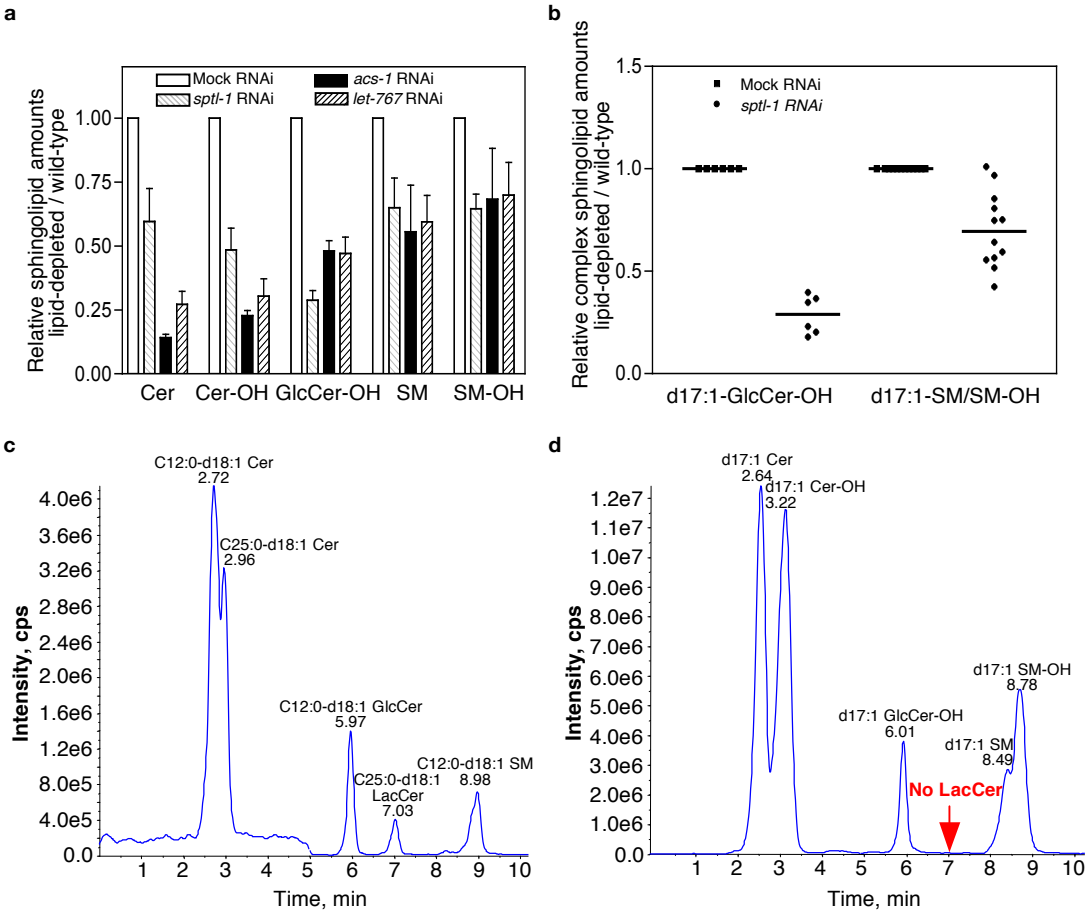

Figure S7 Quantitative and qualitative analysis of selected sphingolipids in sphingolipid- and fatty-acid-biosynthetic-enzyme-depleted and wild-type larvae. **(a)** Relative amounts of C21-26-Cer, -Cer-OH, -GlcCer-OH, C21-23,25-SM and -SM-OH in mock-, *sptl-1-*, *acs-1-* and *let-767(RNAi)* animals (compare Tab.S3; Methods). All of the sphingolipid compounds analyzed were reduced in all three of the fatty-acid- and sphingolipid-biosynthetic-enzyme-depleted animals relative to control. This confirmed the RNAi effect on sphingolipid biosynthesis and suggested that the lipid-biosynthetic-enzyme-dependent polarity phenotype is not caused by a general compensatory distortion of the normal sphigolipid profile. Note, however, that the relative proportions of complex membrane sphingolipids have changed (see b). Error bars indicate SEM, derived from different compounds in each class (distinguished by different fatty-acid chain lengths), wild-type amounts set arbitrarily at 1. Concentrations calculated as described in Fig.6e. **(b)** Among complex membrane sphingolipids, GSLs were consistently more profoundly reduced relative to wild-type than SMs in both sphingolipid- and fatty-acid-biosynthetic-enzyme-depleted RNAi animals (*sptl-1[RNAi]* shown here). Such a change should have consequences for the lipid composition of membranes (see text). Relative amounts of C21-26-GlcCer-OH, and C21-23,25-SM and -SM-OH are plotted. Data acquired and presented as in Fig.6e. **(c, d)** Liquid chromatography-mass spectrometry (LC-MS) profiles of selected sphingolipids in wild-type animals reveal the absence of lactosylceramide (LacCer) in *C. elegans*. Standard mixture (c) contains C25:0-d18:1 lactosylceramide (LacCer) that is missing in *C. elegans* worm extracts (d; indicated in red). LC/MS was performed by scanning the positive mode precursors of 264.4 u for their common d18:1 sphingoid base and 184.2 u optimized for the [M+H]+ fragment for SM in (c) and by scanning the positive mode precursors of 250.3 u for their common d17:1 sphingoid base and 184.2 u for SM in (d; Methods).

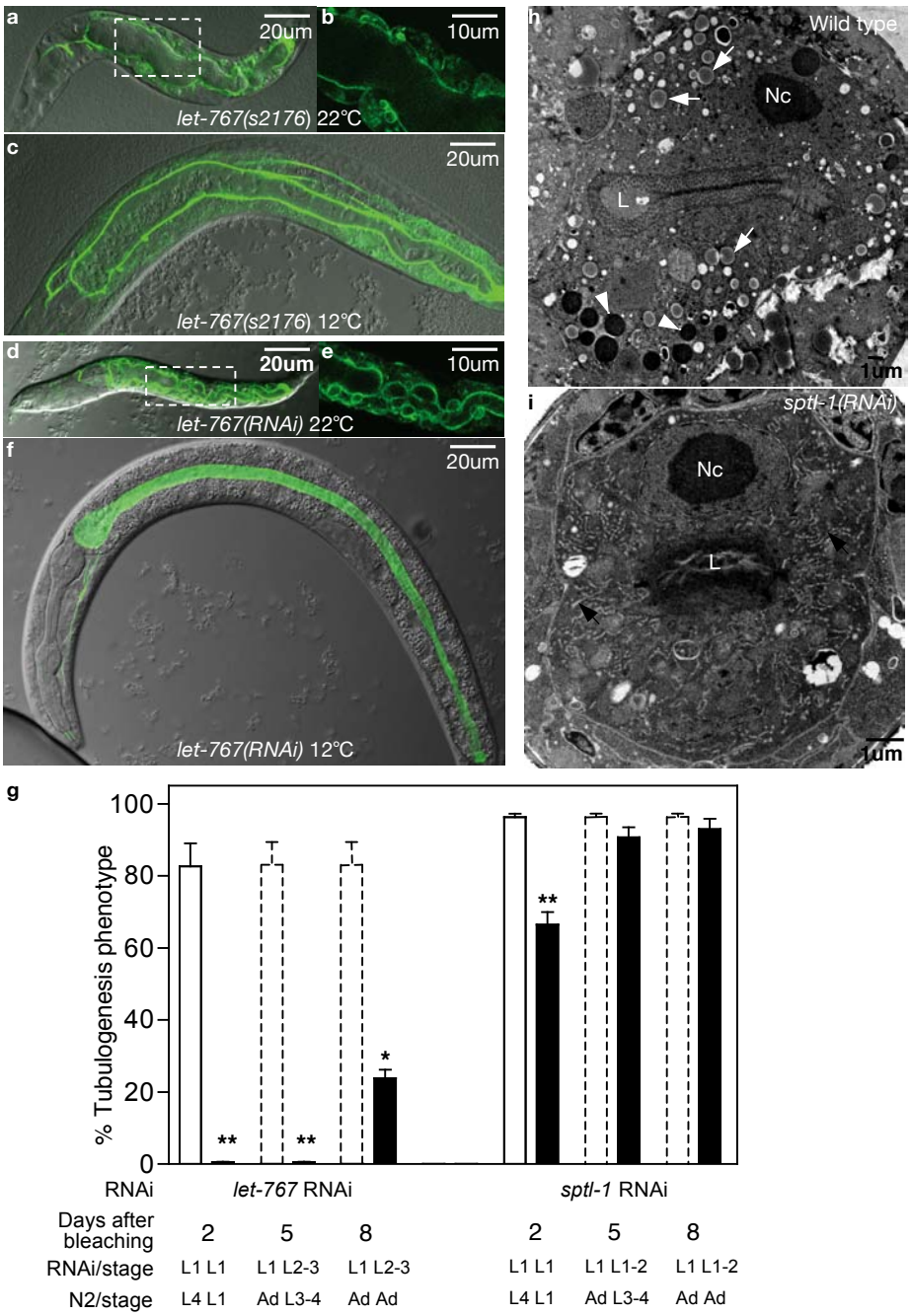

Figure S8 Cold temperature partially rescues polarity conversion and L1 arrest induced by sphingolipid-biosynthesis suppression (compare to Fig.8b). **(a - f)** Nomarski/confocal section overlays of representative *let-767(s2167)* mutants grown at 22^{0}C (a, boxed area magnified in b) or at 12^{0}C (c), and *let-767(RNAi)* animals grown at 22^{0}C (d, boxed area magnified in e) or at 12^{0}C (f). Polarity defects of animals grown at 22^{0}C are absent in those grown at 12^{0}C. Note that cold-treated animals have progressed to L3 stage. Dpy background in *let-767* mutants obscures polarity phenotype (Fig.4). Animals are shown three days (a, b), two days (d, e) and six days (c, f) after bleaching parents (animals hatch ~12 hours post-bleaching; Methods). **(g)** The efficiency of cold rescue is inversely correlated with phenotype severity. *let-767(s2167), let-767(RNAi)* and *sptl-1-(RNAi)* animals have increasingly severe polarity defects (although all induce L1 arrest [Fig.S1]) and are correspondingly less well cold-suppressed (left, strong *let-767(RNAi)* suppression; right, mild *sptl-1-(RNAi)* suppression). Dotted bars indicate populations that displayed the full phenotype at an earlier date and thus were not scored again. Note developmental delay at cold temperature. Corresponding development stage at day scored is indicated beneath bars for RNAi and wild-type animals (N2; larvae: L1 - 4, adult: Ad; days post-bleaching on x-axis). Mean +/- SD is shown, n=4 (N>150 animals per experiment), $^*P<0.05$, $^{**}P<0.01$, two-tailed *t* test. **(h, i)** Vesicle depletion and excess distended ER/Golgi membranes in *sptl-1(RNAi)* L1 intestines. Corresponding whole intestinal cross-sections to Fig.8c TEM micrographs are shown, wild-type (h) and *sptl-1* RNAi (i; see Fig.8c for legend).